

# Asymptotically accurate and locking-free finite element implementation of the refined shell theory

Khanh Chau Le<sup>a,b1</sup> and Hoang-Giang Bui<sup>c</sup>

<sup>a</sup>*Mechanics of Advanced Materials and Structures, Institute for Advanced Study in Technology, Ton Duc Thang University, Ho Chi Minh City, Vietnam*

<sup>b</sup>*Faculty of Civil Engineering, Ton Duc Thang University, Ho Chi Minh City, Vietnam*

<sup>c</sup>*Institute of Material Systems Modeling, Helmholtz-Zentrum Hereon, Geesthacht, Germany*

---

## Abstract

A formulation of the 2D refined shell theory incorporating transverse shear in the rescaled coordinates and angles of rotation is considered. This novel approach provides the first asymptotically accurate and inherently locking-free finite element implementation. Numerical simulations of semi-cylindrical shells demonstrate excellent agreement between the analytical solution, the 2D refined shell theory, and three-dimensional elasticity theory, validating the effectiveness and accuracy of the method.

*Keywords:* refined theory, shells, finite element, asymptotic accuracy, locking-free.

---

## 1. Introduction

Shells, thin-walled structures with curved surfaces, are ubiquitous in engineering, from civil and environmental to mechanical and aerospace applications. Understanding their structural behavior is crucial in designing safe, efficient and resilient structures. When a shell's thickness is significantly smaller than its characteristic radius of curvature and longitudinal size, its deformation can be effectively approximated using functions defined on 2D surface coordinates. Asymptotic analysis, using shell thickness as a model parameter, provides a hypothesis-free and systematic way to derive such 2D

---

<sup>1</sup>Corresponding author. Phone: +84 93 4152458, email: lekhanhchau@tdtu.edu.vn

shell theories from 3D elasticity theory. This rigorous approach, based on the asymptotic analysis of 3D elasticity's strong [1] and weak formulation [2], yields not only the classical shell theory [3, 4] but also various refined shell theories (see [1, 2, 5]).

Accurate modeling of shells, especially concerning transverse shear effects, has driven the development of refined theories. Berdichevsky's pioneering work constructed an asymptotically exact refined shell theory using the variational-asymptotic method (VAM) [6, 7, 2]. This theory maintains the accuracy up to  $O(h/R)$ ,  $O(h/l)$ , and  $O(h^2/l^2)$ , where  $h$ ,  $R$ , and  $l$  represent the shell thickness, curvature radius, and longitudinal deformation scale, respectively. While sharing asymptotic equivalence with Reissner's first-order shear deformation theory (FSDT) for plates [8], Berdichevsky's formulation uniquely provides pointwise accuracy for both displacements and stresses, contrasting with Reissner's integral-based accuracy. The necessity of refined theories is evident from the potential inaccuracies in displacement predictions by classical shell theory [5]. Subsequent efforts have expanded VAM applications to laminated structures [9, 10, 11, 12], often optimizing FSDT parameters for near-asymptotic correctness. Beyond linear elasticity, VAM has been applied to various nonlinear materials [13, 14, 15, 16]. Recent investigations have explored asymptotically exact FSDT for functionally graded plates [17], alongside VAM's utility in dimension reduction, homogenization, and dynamic analyses [18, 19, 20, 21, 22, 23, 24, 25].

The mathematical complexity of 2D refined shell theories often precludes analytical solutions, making finite element implementation crucial for practical problems. However, membrane and shear locking can significantly reduce the reliability [26, 27, 28]. Shear locking arises from the disparity between shear and bending stiffnesses, coupled with much smaller rotations from pure shear versus bending-induced curvature changes. This discrepancy, evident in the variational-asymptotic analysis of the energy functional [2, 29], leads to numerical instability as shell thickness vanishes ( $h \rightarrow 0$ ) with standard low-order elements. Membrane locking stems from the contrast between extension and bending stiffnesses and measures, causing instability due to multiplication of small and large quantities as  $h \rightarrow 0$ .

While sophisticated methods exist to alleviate locking, they often compromise computational efficiency. Reduced and selective integration [30, 31, 32], using different rules for different energy components, is a popular technique but can introduce instability due to rank deficiency and spurious energy modes [33]. Thus, alternative formulations and techniques have been devel-

oped for improved accuracy and stability [34, 35, 36, 37, 28, 38, 39, 40, 41, 42].

Recently, a novel rescaled formulation of FSDT for plates, inherently free from shear locking regardless of discretization or integration, was presented [43]. Numerical simulations demonstrated the asymptotic accuracy of Berdichevsky’s theory for plates using isogeometric elements ensuring  $C^1$ -continuity of primary variables. Building on this foundation, this work extends and pursues two main goals. On one hand, we extend the rescaled formulation to shells, providing a thickness-independent, locking-free approach that boosts efficiency without high-order interpolation or complex integration. On the other hand, and most importantly, we aim for asymptotic accuracy in the first finite element implementation of inherently locking-free Berdichevsky’s refined shell theory. Following [6, 17], this requires  $C^1$ -continuity for both displacements and rotation angles. Numerical simulations of semi-cylindrical shells, compared against analytical and 3D elasticity solutions, validate the achievement of asymptotic accuracy using suitable isogeometric elements.

The paper is structured as follows: Section 2 outlines the 2D refined shell theory and its variational principle. Section 3 details the rescaled, locking-free variational formulation. Section 4 describes the finite element implementation. Section 5 presents numerical examples, including semi-cylindrical shells under internal pressure and a composite structure, and Section 6 concludes the paper.

## 2. 2D refined shell theory: Kinematics and variational principle

Consider a smooth, two-dimensional surface  $\mathcal{S}$  within three-dimensional Euclidean space, bounded by a continuous closed curve  $\partial\mathcal{S}$ . We define a shell volume  $\mathcal{V}$  by constructing line segments of length  $h$ , orthogonal to  $\mathcal{S}$  at each point, with their midpoints on the surface. This definition is valid for sufficiently small shell thickness  $h$ , ensuring no segment intersections. Here,  $\mathcal{S}$  represents the shell’s middle surface, and  $h$  its thickness (Fig. 1).

Mathematically,  $\mathcal{S}$  is represented by the vector equation:

$$\mathbf{z} = \mathbf{r}(x^1, x^2), \tag{1}$$

or, in component form:

$$z^i = r^i(x^\alpha), \quad i = 1, 2, 3; \quad \alpha = 1, 2, \tag{2}$$

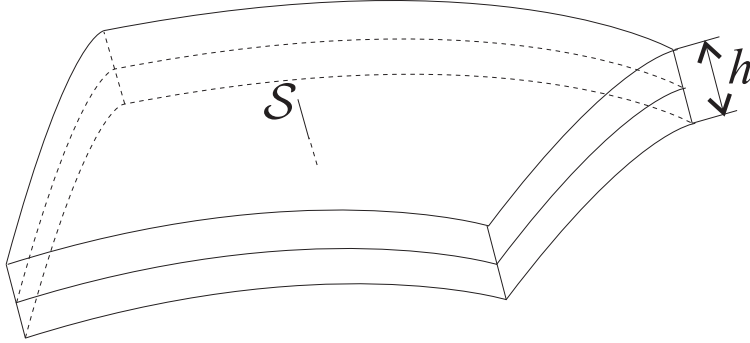


Figure 1: Schematic diagram of a shell segment

where  $\mathbf{z}$  denotes the position vector in a 3D Cartesian system, and  $\mathbf{r}(x^1, x^2)$  is a smooth vector function. Curvilinear coordinates  $x^1$  and  $x^2$  are chosen on  $\mathcal{S}$ , with units of length.

The shell's geometric characteristics are described by the first and second fundamental forms:

$$\begin{aligned} a_{\alpha\beta} &= \mathbf{t}_\alpha \cdot \mathbf{t}_\beta, \\ b_{\alpha\beta} &= -\mathbf{t}_\alpha \cdot \mathbf{n}_{,\beta} = \mathbf{t}_{\alpha,\beta} \cdot \mathbf{n}, \end{aligned} \quad (3)$$

where  $\mathbf{t}_\alpha = \mathbf{r}_{,\alpha}$  are tangent vectors, and  $\mathbf{n}$  is the unit normal vector to  $\mathcal{S}$ , given by:

$$\mathbf{n} = \frac{\mathbf{t}_1 \times \mathbf{t}_2}{|\mathbf{t}_1| |\mathbf{t}_2|}. \quad (4)$$

We utilize Latin indices (1 to 3) for Cartesian coordinates and Greek indices (1 to 2) for surface coordinates. A comma preceding an index signifies partial differentiation.

Within 2D linear kinematics, shell deformation is defined by the displacement vector  $\mathbf{u}(x^1, x^2) = u^i \mathbf{e}_i$ , with  $\mathbf{e}_i$  as Cartesian basis vectors. In the basis  $\{\mathbf{t}_\alpha, \mathbf{n}\}$ , displacement components are:

$$u_\alpha = \mathbf{t}_\alpha \cdot \mathbf{u}, \quad u = \mathbf{n} \cdot \mathbf{u}. \quad (5)$$

The 2D refined shell theory (2D-RST), considering transverse shear, introduces two additional degrees of freedom,  $\varphi_\alpha(x^1, x^2)$ , representing shear-induced rotation angles. The shell's deformation is characterized by: (i) extension measures:

$$\gamma_{\alpha\beta} = r_{,(\alpha}^i u_{i,\beta)} = u_{(\alpha;\beta)} - b_{\alpha\beta} u, \quad (6)$$

(ii) bending measures:

$$\rho_{\alpha\beta} = (n_i u_{i,(\alpha)}^i)_{;\beta)} + b_{(\alpha}^\lambda \varpi_{\beta)\lambda} - \varphi_{(\alpha;\beta)} = u_{;\alpha\beta} + (u_\lambda b_{(\alpha}^\lambda)_{;\beta)} + b_{(\alpha}^\lambda \varpi_{\beta)\lambda} - \varphi_{(\alpha;\beta)}, \quad (7)$$

where

$$\varpi_{\alpha\beta} = \frac{1}{2}(r_{,\beta}^i u_{i,\alpha} - r_{,\alpha}^i u_{i,\beta}) = \frac{1}{2}(u_{\beta,\alpha} - u_{\alpha,\beta}), \quad (8)$$

and (iii) rotation angles  $\varphi_\alpha$ . When  $\varphi_\alpha = 0$ ,  $\rho_{\alpha\beta}$  reduces to classical shell theory bending measures [3, 4]. Parentheses around indices denote symmetrization, and repeated indices imply summation. The metric tensor  $a_{\alpha\beta}$  and its inverse  $a^{\alpha\beta}$  are used to lower or raise surface vector and tensor component indices. Covariant derivatives, indicated by a semicolon in indices, account for basis vector variations in surface tensors. For instance:

$$\begin{aligned} \nabla_\beta u_\alpha &\equiv u_{\alpha;\beta} = u_{\alpha,\beta} - \Gamma_{\alpha\beta}^\lambda u_\lambda, \\ \nabla_\beta u^\alpha &\equiv u_{;\beta}^\alpha = u_{,\beta}^\alpha + \Gamma_{\beta\lambda}^\alpha u^\lambda, \end{aligned} \quad (9)$$

where  $\Gamma_{\alpha\beta}^\lambda$  are Christoffel's symbols:

$$\Gamma_{\alpha\beta}^\lambda = \frac{1}{2}a^{\lambda\mu}(a_{\mu\alpha,\beta} + a_{\mu\beta,\alpha} - a_{\alpha\beta,\mu}). \quad (10)$$

Note the difference in coordinate expressions for covariant derivatives of co- and contravariant vector components in (9). These definitions extend to tensor components [29].

The 2D-RST for linearly elastic, homogeneous shells is based on a variational principle [2, 6]. It states that the actual displacement field and rotation angles minimize the two-dimensional average energy functional

$$J[\mathbf{u}, \varphi_\alpha] = \int_S \Phi(\gamma_{\alpha\beta}, \rho_{\alpha\beta}, \varphi_\alpha) d\omega - \mathcal{A}_{\text{ext}} \quad (11)$$

among all admissible displacement fields and rotation angles that satisfy the kinematic boundary conditions. Here,  $d\omega = \sqrt{a}dx^1dx^2$  is the area element, and  $a = \det a_{\alpha\beta}$ . The two-dimensional energy density  $\Phi(\gamma_{\alpha\beta}, \rho_{\alpha\beta}, \varphi_\alpha)$  comprises three contributions, namely, (i)  $\Phi_{\text{cl}}(\gamma_{\alpha\beta}, \rho_{\alpha\beta})$ : energy density of classical shell theory, (ii)  $\Phi_{\text{gc}}(\gamma_{\alpha\beta}, \rho_{\alpha\beta})$ : geometric correction energy, (iii)  $\Phi_{\text{sc}}(\varphi_\alpha)$ : shear correction energy. Thus:

$$\Phi(\gamma_{\alpha\beta}, \rho_{\alpha\beta}, \varphi_\alpha) = \Phi_{\text{cl}}(\gamma_{\alpha\beta}, \rho_{\alpha\beta}) + \Phi_{\text{gc}}(\gamma_{\alpha\beta}, \rho_{\alpha\beta}) + \Phi_{\text{sc}}(\varphi_\alpha). \quad (12)$$

These are explicitly given by:

$$\begin{aligned}
\Phi_{\text{cl}}(\gamma_{\alpha\beta}, \rho_{\alpha\beta}) &= \mu h \left[ \sigma(\gamma_\alpha^\alpha)^2 + \gamma_{\alpha\beta}\gamma^{\alpha\beta} \right] + \frac{\mu h^3}{12} \left[ \sigma(\rho_\alpha^\alpha)^2 + \rho_{\alpha\beta}\rho^{\alpha\beta} \right], \\
\Phi_{\text{gc}}(\gamma_{\alpha\beta}, \rho_{\alpha\beta}) &= -\frac{\mu h^3}{3} \left[ \rho^{\alpha\beta} b_\alpha^\lambda \gamma_{\beta\lambda} + \sigma \rho^{\alpha\beta} b_{\alpha\beta} \gamma_\lambda^\lambda + \frac{3}{5} \sigma \rho_\lambda^\lambda b^{\alpha\beta} \gamma_{\alpha\beta} \right. \\
&\quad \left. + \sigma \left( \frac{6}{5} \sigma - 1 \right) \rho_\lambda^\lambda H \gamma_\mu^\mu \right], \\
\Phi_{\text{sc}}(\varphi_\alpha) &= \frac{5}{12} \mu h a^{\alpha\beta} \varphi_\alpha \varphi_\beta,
\end{aligned} \tag{13}$$

where  $\lambda$  and  $\mu$  are Lamé's constants,  $\sigma = \frac{\lambda}{\lambda+2\mu} = \frac{\nu}{1-\nu}$ , and  $b_\alpha^\lambda = b_\alpha^\lambda - H\delta_\alpha^\lambda$  is the deviator of the second quadratic form, with  $H = b_\alpha^\alpha/2$  being the mean curvature. The work done by external loads is expressed as

$$\begin{aligned}
\mathcal{A}_{\text{ext}} = \int_S \left[ (f_i - hH g_i) u^i + \frac{h}{2} g_\alpha (u_{,\alpha} + b_\alpha^\lambda u_\lambda) - \frac{\sigma h}{2} (g + \frac{1}{6} h f_{;\alpha}^\alpha) \gamma_\beta^\beta \right. \\
\left. - \frac{1}{10} \sigma h^2 (f + \frac{1}{12} h g_{;\alpha}^\alpha) \rho_\beta^\beta - \frac{1}{12} g^\alpha h \varphi_\alpha \right] d\omega, \tag{14}
\end{aligned}$$

where

$$\begin{aligned}
f_i &= \tau_i|_{x_3=h/2} + \tau_i|_{x_3=-h/2}, & f_\alpha &= f_i r_{,\alpha}^i, & f &= f_i n^i, \\
g_i &= \tau_i|_{x_3=h/2} - \tau_i|_{x_3=-h/2}, & g_\alpha &= g_i r_{,\alpha}^i, & g &= g_i n^i,
\end{aligned} \tag{15}$$

with  $\tau_i$  representing the Cartesian components of the traction vector.

This 2D refined shell theory, by maintaining asymptotic accuracy up to  $O(h/R)$  and  $O(h^2/l^2)$ , extends reliable analysis to shells of moderate thickness, where  $R$  and  $l$  denote the characteristic radius of curvature and longitudinal deformation length-scale, respectively [6, 2].

### 3. Rescaled formulation

The finite element (FE) implementation of the 2D variational problem (Eq. (11)) presents challenges due to the differing orders of magnitude between bending and shear stiffnesses. Shear stiffness, significantly exceeding bending stiffness by two orders relative to shell thickness  $h$ , can cause numerical instability (shear locking) when multiplied by small rotation angles as  $h$  decreases. A similar issue, membrane locking, arises from the contrast between extension and bending stiffnesses, and their respective measures.

To address these challenges, we introduce new unknown functions,

$$\psi_\alpha = -n_i u_{,\alpha}^i + \varphi_\alpha = -u_{,\alpha} - u_\lambda b_\alpha^\lambda + \varphi_\alpha, \quad (16)$$

representing the total rotation angles of transverse fibers resulting from both bending and shear, such that

$$\begin{aligned} \rho_{\alpha\beta} &= -\psi_{(\alpha;\beta)} + b_{(\alpha}^\lambda \varpi_{\beta)\lambda}, \\ \varphi_\alpha &= u_{,\alpha} + u_\lambda b_\alpha^\lambda + \psi_\alpha. \end{aligned} \quad (17)$$

Consequently, the functional in Eq. (11) is reformulated with these unknowns as

$$J[\mathbf{u}, \psi_\alpha] = \int_{\mathcal{S}} \Phi(\gamma_{\alpha\beta}, \rho_{\alpha\beta}, u_{,\alpha} + u_\lambda b_\alpha^\lambda + \psi_\alpha) d\omega - \mathcal{A}_{\text{ext}}, \quad (18)$$

where function  $\Phi$  of three arguments remains the same as in (12), while  $\rho_{\alpha\beta}$  should be taken from (17)<sub>1</sub>. To avoid the membrane- and shear-locking effects, we aim to make the problem independent of  $h$ , ensuring that extension, bending, and shear stiffnesses have comparable orders of magnitude. We introduce rescaled coordinates:

$$\bar{z}^i = \frac{z^i}{h}, \quad \bar{x}^\alpha = \frac{x^\alpha}{h}, \quad (19)$$

and express Eq. (2) as

$$\bar{z}^i = \bar{r}^i(\bar{x}^\alpha), \quad (20)$$

where  $\bar{r}^i(\bar{x}^\alpha) = r^i(x^\alpha)/h$ . This rescaling renders the left-hand side of (19) dimensionless. Importantly, the basis vectors and unit normal vector are unaffected, preserving the metric tensor and its inverse. Specifically,

$$\bar{\mathbf{r}}_{,\bar{\alpha}} = \frac{\partial \bar{\mathbf{r}}}{\partial \bar{x}^\alpha} = \frac{\partial(\mathbf{r}/h)}{\partial(x^\alpha/h)} = \mathbf{r}_{,\alpha}, \quad (21)$$

thus  $\bar{\mathbf{n}} = \mathbf{n}$ .

Displacements are unchanged, but to reflect their dependence on the new base  $\{\bar{\mathbf{r}}_{,\bar{\alpha}}, \bar{\mathbf{n}}\}$  and argument  $\bar{x}^\alpha$ , they are denoted as:

$$\bar{u}_{\bar{\alpha}}(\bar{x}^\alpha) = u_\alpha(x^\alpha), \quad \bar{u}(\bar{x}^\alpha) = u(x^\alpha). \quad (22)$$

The second fundamental form of the surface transforms as

$$\bar{b}_{\bar{\alpha}\bar{\beta}} = \bar{\mathbf{r}}_{,\bar{\alpha}\bar{\beta}} \cdot \bar{\mathbf{n}} = h \mathbf{r}_{,\alpha\beta} \cdot \mathbf{n} = h b_{\alpha\beta}, \quad (23)$$

resulting in scaled principal radii of curvature  $\bar{R}_1 = R_1/h$  and  $\bar{R}_2 = R_2/h$ . Partial derivatives with respect to  $\bar{x}^\alpha$  are related to those with respect to  $x^\alpha$  by

$$\frac{\partial}{\partial \bar{x}^\alpha} = h \frac{\partial}{\partial x^\alpha}, \quad (\cdot)_{,\bar{\alpha}} = h(\cdot)_{,\alpha}. \quad (24)$$

From Eq. (10), the scaled Christoffel symbols are related to the original ones by

$$\bar{\Gamma}_{\bar{\alpha}\bar{\beta}}^{\bar{\lambda}} = \frac{1}{2} \bar{a}^{\bar{\lambda}\bar{\mu}} (\bar{a}_{\bar{\mu}\bar{\alpha},\bar{\beta}} + \bar{a}_{\bar{\mu}\bar{\beta},\bar{\alpha}} - \bar{a}_{\bar{\alpha}\bar{\beta},\bar{\mu}}) = \frac{1}{2} h a^{\lambda\mu} (a_{\mu\alpha,\beta} + a_{\mu\beta,\alpha} - a_{\alpha\beta,\mu}) = h \Gamma_{\alpha\beta}^{\lambda}. \quad (25)$$

Therefore, covariant derivatives with respect to  $\bar{x}^\alpha$  are also related to those with respect to  $x^\alpha$  by

$$\bar{\nabla}_{\bar{\alpha}} = h \nabla_{\alpha}, \quad (\cdot)_{;\bar{\alpha}} = h(\cdot)_{;\alpha}. \quad (26)$$

For rotation angles, we introduce

$$\bar{\psi}_{\bar{\alpha}} = h \psi_{\alpha}, \quad (27)$$

with dimensions of length, representing longitudinal displacements of the shell's positive face [6].

Applying the scaling rules (19), (22), and (27), we obtain the following relationships between original and rescaled quantities:

$$\begin{aligned} \gamma_{\alpha\beta} &= \frac{1}{h} \bar{\gamma}_{\bar{\alpha}\bar{\beta}}, & \rho_{\alpha\beta} &= \frac{1}{h^2} \bar{\rho}_{\bar{\alpha}\bar{\beta}}, \\ u_{,\alpha} + u_{\lambda} b_{\alpha}^{\lambda} + \psi_{\alpha} &= \frac{1}{h} (\bar{u}_{,\bar{\alpha}} + \bar{u}_{\bar{\lambda}} \bar{b}_{\bar{\alpha}}^{\bar{\lambda}} + \bar{\psi}_{\bar{\alpha}}), \\ d\omega &= \sqrt{a} dx^1 dx^2 = h^2 \sqrt{\bar{a}} d\bar{x}^1 d\bar{x}^2 = h^2 d\bar{\omega}, \end{aligned} \quad (28)$$

where

$$\begin{aligned} \bar{\gamma}_{\bar{\alpha}\bar{\beta}} &= \bar{u}_{(\bar{\alpha};\bar{\beta})} - \bar{b}_{\bar{\alpha}\bar{\beta}}^{\bar{\lambda}} \bar{u}_{\bar{\lambda}}, \\ \bar{\rho}_{\bar{\alpha}\bar{\beta}} &= -\bar{\psi}_{(\bar{\alpha};\bar{\beta})} + \bar{b}_{(\bar{\alpha}}^{\bar{\lambda}} \bar{\omega}_{\bar{\beta})\bar{\lambda}}, \end{aligned} \quad (29)$$

and

$$\bar{\omega}_{\bar{\alpha}\bar{\beta}} = \frac{1}{2} (\bar{u}_{\bar{\beta},\bar{\alpha}} - \bar{u}_{\bar{\alpha},\bar{\beta}}). \quad (30)$$

Substituting Eqs. (28) into the energy functional (18) gives a form with rescaled quantities:

$$J[\bar{\mathbf{u}}, \bar{\psi}_{\bar{\alpha}}] = \mu h \int_{\bar{S}} \bar{\Phi}(\bar{\gamma}_{\bar{\alpha}\bar{\beta}}, \bar{\rho}_{\bar{\alpha}\bar{\beta}}, \bar{u}_{,\bar{\alpha}} + \bar{u}_{\bar{\lambda}} \bar{b}_{\bar{\alpha}}^{\bar{\lambda}} + \bar{\psi}_{\bar{\alpha}}) d\bar{\omega} - \mathcal{A}_{\text{ext}}. \quad (31)$$



Here  $\bar{\mathcal{S}} = \{(\bar{x}_1, \bar{x}_2) \mid (x_1, x_2) \in \mathcal{S}\}$  denotes the rescaled 2D domain, while the rescaled energy density,  $\bar{\Phi}(\bar{\gamma}_{\alpha\beta}, \bar{\rho}_{\alpha\beta}, \bar{u}_{,\alpha} + \bar{u}_{\bar{\lambda}}\bar{b}_{\alpha}^{\bar{\lambda}} + \bar{\psi}_{\alpha})$ , is the sum of three contributions

$$\begin{aligned}\bar{\Phi}_{\text{cl}}(\bar{\gamma}_{\alpha\beta}, \bar{\rho}_{\alpha\beta}) &= \sigma(\bar{\gamma}_{\alpha}^{\alpha})^2 + \bar{\gamma}_{\alpha\beta}\bar{\gamma}^{\alpha\beta} + \frac{1}{12}\left[\sigma(\bar{\rho}_{\alpha}^{\alpha})^2 + \bar{\rho}_{\alpha\beta}\bar{\rho}^{\alpha\beta}\right], \\ \bar{\Phi}_{\text{gc}}(\bar{\gamma}_{\alpha\beta}, \bar{\rho}_{\alpha\beta}) &= -\frac{1}{3}\left[\bar{\rho}^{\alpha\beta}\bar{b}_{\alpha}^{\bar{\lambda}}\bar{\gamma}_{\beta\bar{\lambda}} + \sigma\bar{\rho}^{\alpha\beta}\bar{b}_{\alpha\beta}\bar{\gamma}_{\bar{\lambda}}^{\bar{\lambda}} + \frac{3}{5}\sigma\bar{\rho}_{\bar{\lambda}}^{\bar{\lambda}}\bar{b}^{\alpha\beta}\bar{\gamma}_{\alpha\beta}\right. \\ &\quad \left. + \sigma\left(\frac{6}{5}\sigma - 1\right)\bar{\rho}_{\bar{\lambda}}^{\bar{\lambda}}\bar{H}\bar{\gamma}_{\bar{\mu}}^{\bar{\mu}}\right], \\ \bar{\Phi}_{\text{sc}}(\bar{u}_{,\alpha} + \bar{u}_{\bar{\lambda}}\bar{b}_{\alpha}^{\bar{\lambda}} + \bar{\psi}_{\alpha}) &= \frac{5}{12}\bar{a}^{\alpha\beta}(\bar{u}_{,\alpha} + \bar{u}_{\bar{\lambda}}\bar{b}_{\alpha}^{\bar{\lambda}} + \bar{\psi}_{\alpha})(\bar{u}_{,\beta} + \bar{u}_{\bar{\mu}}\bar{b}_{\beta}^{\bar{\mu}} + \bar{\psi}_{\beta})\end{aligned}\quad (32)$$

similar to (12). The work of external forces becomes

$$\begin{aligned}\mathcal{A}_{\text{ext}} &= h^2 \int_{\mathcal{S}} \left[ (f_i - \bar{H}g_i)\bar{u}^i + \frac{1}{2}g^{\alpha}(\bar{u}_{,\alpha} + \bar{u}_{\bar{\lambda}}\bar{b}_{\alpha}^{\bar{\lambda}}) - \frac{\sigma}{2}(g + \frac{1}{6}f_{;\alpha}^{\alpha})\bar{\gamma}_{\beta}^{\beta} \right. \\ &\quad \left. + \frac{1}{10}\sigma(f + \frac{1}{12}g_{;\alpha}^{\alpha})\bar{\psi}_{;\beta}^{\beta} - \frac{1}{12}g^{\alpha}(\bar{u}_{,\alpha} + \bar{u}_{\bar{\lambda}}\bar{b}_{\alpha}^{\bar{\lambda}} + \bar{\psi}_{\alpha}) \right] d\bar{\omega}\end{aligned}\quad (33)$$

Since scaling a functional by a constant does not alter its minimizer, we further simplify (31) by dividing by  $\mu h$ . The minimization problem becomes

$$\bar{J}[\bar{\mathbf{u}}, \bar{\psi}_{\alpha}] = \int_{\bar{\mathcal{S}}} \bar{\Phi}(\bar{\gamma}_{\alpha\beta}, \bar{\rho}_{\alpha\beta}, \bar{u}_{,\alpha} + \bar{u}_{\bar{\lambda}}\bar{b}_{\alpha}^{\bar{\lambda}} + \bar{\psi}_{\alpha}) d\bar{\omega} - \bar{\mathcal{A}}_{\text{ext}} \rightarrow \min_{\bar{u}_{\alpha}, \bar{u}, \bar{\psi}_{\alpha}}, \quad (34)$$

where

$$\begin{aligned}\bar{\mathcal{A}}_{\text{ext}} &= \int_{\mathcal{S}} \left[ (\bar{f}_i - \bar{H}\bar{g}_i)\bar{u}^i + \frac{1}{2}\bar{g}^{\alpha}(\bar{u}_{,\alpha} + \bar{u}_{\bar{\lambda}}\bar{b}_{\alpha}^{\bar{\lambda}}) - \frac{\sigma}{2}(\bar{g} + \frac{1}{6}\bar{f}_{;\alpha}^{\alpha})\bar{\gamma}_{\beta}^{\beta} \right. \\ &\quad \left. + \frac{1}{10}\sigma(\bar{f} + \frac{1}{12}\bar{g}_{;\alpha}^{\alpha})\bar{\psi}_{;\beta}^{\beta} - \frac{1}{12}\bar{g}^{\alpha}(\bar{u}_{,\alpha} + \bar{u}_{\bar{\lambda}}\bar{b}_{\alpha}^{\bar{\lambda}} + \bar{\psi}_{\alpha}) \right] d\bar{\omega},\end{aligned}\quad (35)$$

and

$$\bar{f}_i = \frac{hf_i}{\mu}, \quad \bar{g}_i = \frac{hg_i}{\mu}. \quad (36)$$

Consequently, both  $\bar{f}_i$  and  $\bar{g}_i$  scale with shell thickness  $h$  and strain  $\varepsilon = \max\{f_i/\mu, g_i/\mu\}$ . Since all three stiffnesses (extension, bending, and shear) in the rescaled functional (34) are  $O(1)$ , the minimizer is  $O(\bar{f}_i, \bar{g}_i)$  times a function depending on the characteristic size of  $\bar{\mathcal{S}}$ . Returning to original functions, extension measures  $\gamma_{\alpha\beta}$  and rotation angles  $\psi_{\alpha}$  are  $O(\varepsilon)$  (with

$\varphi_\alpha$  smaller [29, 2]), while bending measures  $\rho_{\alpha\beta}$  are  $O(\varepsilon/h)$ . The rescaled problem (34) avoids membrane and shear locking.

To solve problem (34), boundary conditions must be specified. Typically, we assume a portion of the shell's edge,  $\bar{\partial}_k$ , is clamped, requiring the admissible functions to satisfy the following kinematic conditions:

$$\bar{u}_{\bar{\alpha}} = 0, \quad \bar{u} = 0, \quad \bar{\psi}_{\bar{\alpha}} = 0 \quad \text{at } \bar{\partial}_k. \quad (37)$$

For a simply supported remaining edge  $\bar{\partial}_s$ , kinematical conditions  $\bar{u}_{\bar{\alpha}} = 0$ ,  $\bar{u} = 0$ , and  $\bar{\psi}_{\bar{\alpha}}\bar{\tau}^{\bar{\alpha}} = 0$  are enforced, while  $\bar{\psi}_{\bar{\alpha}}\bar{\nu}^{\bar{\alpha}}$  is allowed to vary freely, where  $\bar{\tau}^{\bar{\alpha}}$  and  $\bar{\nu}^{\bar{\alpha}}$  are the components of the surface tangential and normal unit vectors on  $\bar{\partial}_s$ , respectively. On a free edge  $\bar{\partial}_s$ , no constraints are imposed on  $\bar{u}_{\bar{\alpha}}$ ,  $\bar{u}$  and  $\bar{\psi}_{\bar{\alpha}}$ . Beyond these typical cases, Section 5 explores additional boundary conditions to validate our FE implementation.

After obtaining the solution, the theory's asymptotic accuracy is assessed by comparing the true average displacement with 3D elasticity results. According to [6],  $\bar{u}_{\bar{\alpha}}$  represent the true average tangential displacements. The true average normal displacement is obtained by correcting the normal displacement:

$$\check{u} = u + \frac{h^2\sigma}{60}a^{\alpha\beta}\rho_{\alpha\beta} = \bar{u} + \frac{\sigma}{60}\bar{a}^{\bar{\alpha}\bar{\beta}}(-\bar{\psi}_{(\bar{\alpha};\bar{\beta})} + \bar{b}_{(\bar{\alpha}}^{\bar{\lambda}}\bar{\omega}_{\bar{\beta})\bar{\lambda}}). \quad (38)$$

Since  $\varphi_\alpha$  also depends on first derivatives of  $u$ , we seek solutions where  $\bar{u}_{\bar{\alpha}}$ ,  $\bar{u}$ , and  $\bar{\psi}_{\bar{\alpha}}$  are  $C^1$ -functions for accurate computations and comparisons. Asymptotic accuracy is confirmed by agreement up to  $O(h/R)$  and  $O(h^2/l^2)$  between functions  $\bar{u}_{\bar{\alpha}}$ ,  $\bar{u}$ , and  $\bar{\psi}_{\bar{\alpha}}$  found by the 2D refined shell theory with

$$r_{,\alpha}^i \langle w_i(x^\alpha, x^3) \rangle, \quad n^i \langle w_i(x^\alpha, x^3) \rangle, \quad \text{and} \quad r_{,\alpha}^i \langle w_i(x^\alpha, x^3)x^3 \rangle / (h^2/12), \quad (39)$$

where  $\langle \cdot \rangle \equiv \frac{1}{h} \int_{-h/2}^{h/2} \cdot dx^3$  denotes the averaging over the shell's thickness and  $w_i(x^\alpha, x^3)$  are the displacements computed by the 3D exact theory of elasticity.

## 4. Finite element implementation

### 4.1. Weak and strong formulations

In this Section and the theoretical portion of the subsequent Section, we will use rescaled coordinates and quantities exclusively. For brevity, overbars will be omitted.

Taking the first variation of the functional (Eq. (34)), a necessary condition for its minimizer is that the virtual work of internal forces equals the virtual work of external forces:

$$\int_S \left[ n^{\alpha\beta} \delta\gamma_{\alpha\beta} + m^{\alpha\beta} \delta\rho_{\alpha\beta} + q^\alpha (\delta u_{,\alpha} + b_\alpha^\lambda \delta u_\lambda + \delta\psi_\alpha) \right] d\omega = \delta\mathcal{A}_{\text{ext}}, \quad (40)$$

where the membrane forces  $n^{\alpha\beta}$ , bending moments  $m^{\alpha\beta}$ , and shear forces  $q^\alpha$  are dual to  $\gamma_{\alpha\beta}$ ,  $\rho_{\alpha\beta}$  and  $\varphi_\alpha$ , respectively. These are defined as:

$$\begin{aligned} n^{\alpha\beta} &= \frac{\partial\Phi}{\partial\gamma_{\alpha\beta}} = 2(\sigma\gamma_\lambda^\lambda a^{\alpha\beta} + \gamma^{\alpha\beta}) - \frac{1}{3} \left[ \rho^{(\alpha\lambda} b_\lambda'^{\beta)} + \sigma a^{\alpha\beta} (b_{\mu\nu} \rho^{\mu\nu} \right. \\ &\quad \left. + \left(\frac{6}{5}\sigma - 1\right) H \rho_\lambda^\lambda \right) + \frac{3}{5} \sigma \rho_\lambda^\lambda b^{\alpha\beta} \right], \\ m^{\alpha\beta} &= \frac{\partial\Phi}{\partial\rho_{\alpha\beta}} = \frac{1}{6} (\sigma \rho_\lambda^\lambda a^{\alpha\beta} + \rho^{\alpha\beta}) - \frac{1}{3} \left[ \gamma^{(\alpha\lambda} b_\lambda'^{\beta)} + \sigma a^{\alpha\beta} \left( \frac{3}{5} b_{\mu\nu} \gamma^{\mu\nu} \right. \right. \\ &\quad \left. \left. + \left(\frac{6}{5}\sigma - 1\right) H \gamma_\lambda^\lambda \right) + \sigma \gamma_\lambda^\lambda b^{\alpha\beta} \right], \\ q^\alpha &= \frac{\partial\Phi}{\partial\varphi_\alpha} = \frac{5}{6} a^{\alpha\beta} (u_{,\beta} + b_\beta^\lambda u_\lambda + \psi_\beta). \end{aligned} \quad (41)$$

The virtual work of external forces is:

$$\begin{aligned} \delta\mathcal{A}_{\text{ext}} &= \int_S \left[ (f^\alpha - H g^\alpha) \delta u_\alpha + (f - H g) \delta u + \frac{1}{2} g^\alpha (\delta u_{,\alpha} + b_\alpha^\lambda \delta u_\lambda) - \frac{\sigma}{2} \left( g + \frac{1}{6} f_{;\lambda}^\lambda \right) a^{\alpha\beta} \delta\gamma_{\alpha\beta} \right. \\ &\quad \left. + \frac{\sigma}{10} \left( f + \frac{1}{12} g_{;\lambda}^\lambda \right) a^{\alpha\beta} \delta\psi_{\alpha;\beta} - \frac{1}{12} g^\alpha (\delta u_{,\alpha} + b_\alpha^\lambda \delta u_\lambda + \delta\psi_\alpha) \right] d\omega. \end{aligned} \quad (42)$$

Introducing the notations

$$\begin{aligned} \delta W^m &= \int_S n^{\alpha\beta} \delta\gamma_{\alpha\beta} d\omega = \int_S d\omega \left\{ 2(\sigma\gamma_\lambda^\lambda a^{\alpha\beta} + \gamma^{\alpha\beta}) - \frac{1}{3} \left[ \rho^{(\alpha\lambda} b_\lambda'^{\beta)} + \sigma a^{\alpha\beta} (b_{\mu\nu} \rho^{\mu\nu} \right. \right. \\ &\quad \left. \left. + \left(\frac{6}{5}\sigma - 1\right) H \rho_\lambda^\lambda \right) + \frac{3}{5} \sigma \rho_\lambda^\lambda b^{\alpha\beta} \right] \right\} (\delta u_{(\alpha;\beta)} - b_{\alpha\beta} \delta u) d\omega, \end{aligned} \quad (43)$$

$$\begin{aligned} \delta W^b &= \int_S m^{\alpha\beta} \delta\rho_{\alpha\beta} d\omega = \int_S d\omega \left\{ \frac{1}{6} (\sigma \rho_\lambda^\lambda a^{\alpha\beta} + \rho^{\alpha\beta}) - \frac{1}{3} \left[ \gamma^{(\alpha\lambda} b_\lambda'^{\beta)} + \sigma a^{\alpha\beta} \left( \frac{3}{5} b_{\mu\nu} \gamma^{\mu\nu} \right. \right. \right. \\ &\quad \left. \left. + \left(\frac{6}{5}\sigma - 1\right) H \gamma_\lambda^\lambda \right) + \sigma \gamma_\lambda^\lambda b^{\alpha\beta} \right] \right\} (-\delta\psi_{(\alpha;\beta)} + b_{(\alpha}^\lambda \delta\varpi_{\beta)\lambda}) d\omega, \end{aligned} \quad (44)$$

and

$$\delta W^s = \int_{\mathcal{S}} q^\alpha \delta \varphi_\alpha \, d\omega = \int_{\mathcal{S}} a^{\alpha\beta} (u_{,\beta} + b_\beta^\lambda u_\lambda + \psi_\beta) (\delta u_{,\alpha} + b_\alpha^\mu \delta u_\mu + \delta \psi_\alpha) \, d\omega, \quad (45)$$

for the virtual work of membrane forces, bending moments, and shear forces, respectively, Eq. (40) becomes:

$$\delta W^m + \delta W^b + \delta W^s = \delta \mathcal{A}_{\text{ext}}. \quad (46)$$

Let  $\mathcal{K} = \{(v, v_\alpha, \chi_\alpha) \mid (v, v_\alpha, \chi_\alpha)|_{\partial_k} = 0\}$  be the space of kinematically admissible functions. The weak formulation of the refined shell theory states that for given  $f, f^\alpha, g, g^\alpha$  find  $(u, u_\alpha, \psi_\alpha) \in \mathcal{K}$  such that Eq. (46) is satisfied for all  $(\delta u, \delta u_\alpha, \delta \psi_\alpha) \in \mathcal{K}$ . Looking at the integrals (43)-(45) we see that, for this weak formulation to make sense, the admissible functions should belong at least to the Sobolev's space of square integrable functions with the square integrable first derivatives,  $H^1(\mathcal{S})$ . However, since the desired asymptotic accuracy of FSDT may require higher smoothness of  $u, u_\alpha$ , and  $\psi_\alpha$ , the continuity assumption in  $\mathcal{K}$  still remains unspecified.

For completeness, we also present the strong formulation of the problem. Assuming  $u, u_\alpha$ , and  $\psi_\alpha$  are twice differentiable, we integrate Eq. (40) by parts, yielding:

$$\begin{aligned} & \int_{\mathcal{S}} \left[ -n_{;\beta}^{\alpha\beta} \delta u_\alpha - b_{\alpha\beta} n^{\alpha\beta} \delta u + m_{;\beta}^{\alpha\beta} \delta \psi_\alpha - (m^{\lambda[\alpha} b_\lambda^{\beta]})_{;\beta} \delta u_\alpha - q_{;\alpha}^\alpha \delta u + b_\beta^\alpha q^\beta \delta u_\alpha \right. \\ & \left. + q^\alpha \delta \psi_\alpha \right] \, d\omega + \int_{\partial_s} \left[ n^{\alpha\beta} \nu_\beta \delta u_\alpha - m^{\alpha\beta} \nu_\beta \delta \psi_\alpha + m^{\lambda[\alpha} b_\lambda^{\beta]} \nu_\beta \delta u_\alpha + q^\alpha \nu_\alpha \delta u \right] \, ds \\ & = \int_{\mathcal{S}} \left[ (f^\alpha - H g^\alpha) \delta u_\alpha + (f - H g) \delta u - \frac{5}{12} g_{;\alpha}^\alpha \delta u + \frac{1}{2} g^\beta b_\beta^\alpha \delta u_\alpha + \frac{\sigma}{2} (g + \frac{1}{6} f_{;\lambda}^\lambda)_{;\beta} a^{\alpha\beta} \delta u_\alpha \right. \\ & \left. + \sigma H (g + \frac{1}{6} f_{;\lambda}^\lambda) \delta u - \frac{\sigma}{10} (f + \frac{1}{12} g_{;\lambda}^\lambda)_{;\beta} a^{\alpha\beta} \delta \psi_\alpha - \frac{1}{12} g^\beta b_\beta^\alpha \delta u_\alpha - \frac{1}{12} g^\alpha \delta \psi_\alpha \right] \, d\omega \\ & \left. + \int_{\partial_s} \left[ \frac{5}{12} g^\alpha \nu_\alpha \delta u - \frac{\sigma}{2} (g + \frac{1}{6} f_{;\lambda}^\lambda) \nu_\beta a^{\alpha\beta} \delta u_\alpha + \frac{\sigma}{10} (f + \frac{1}{12} g_{;\lambda}^\lambda) \nu_\beta a^{\alpha\beta} \delta \psi_\alpha \right] \, ds. \right. \end{aligned} \quad (47)$$

Here, square brackets enclosing indices denote anti-symmetrization:  $t^{[\alpha\beta]} = \frac{1}{2}(t^{\alpha\beta} - t^{\beta\alpha})$ . Vector  $\nu_\alpha$  represents the outward surface normal to  $\partial\mathcal{S}$ , and  $ds$  is the length element. We assume the remaining portion of the shell edge, denoted by  $\partial_s$ , is free. Due to the arbitrariness of the variations  $\delta u_\alpha, \delta \psi_\alpha$ , and

$\delta u$  in  $\mathcal{S}$  and on  $\partial_s$ , we obtain the following second-order partial differential equations from Eq. (47):

$$\begin{aligned}
-t_{;\beta}^{\alpha\beta} + b_{\beta}^{\alpha} q^{\beta} &= f^{\alpha} - H g^{\alpha} + \frac{1}{2} g^{\beta} b_{\beta}^{\alpha} + \frac{\sigma}{2} (g + \frac{1}{6} f_{;\lambda}^{\lambda})_{;\beta} a^{\alpha\beta} - \frac{1}{12} g^{\beta} b_{\beta}^{\alpha} \\
m_{;\beta}^{\alpha\beta} + q^{\alpha} &= -\frac{\sigma}{10} (f + \frac{1}{12} g_{;\lambda}^{\lambda})_{;\beta} a^{\alpha\beta} - \frac{1}{12} g^{\alpha}, \\
-q_{;\alpha}^{\alpha} - b_{\alpha\beta} n^{\alpha\beta} &= f - H g - \frac{5}{12} g_{;\alpha}^{\alpha} + \sigma H (g + \frac{1}{6} f_{;\lambda}^{\lambda}),
\end{aligned} \tag{48}$$

where  $t^{\alpha\beta} = n^{\alpha\beta} + m^{\lambda[\alpha} b_{\lambda}^{\beta]}$ . These equations are subject to the kinematic boundary conditions (Eq. (37)) on  $\partial_k$  and the following natural boundary conditions on  $\partial_s$ :

$$\begin{aligned}
t^{\alpha\beta} \nu_{\beta} &= -\frac{\sigma}{2} (g + \frac{1}{6} f_{;\lambda}^{\lambda}) \nu_{\beta} a^{\alpha\beta}, \\
-m^{\alpha\beta} \nu_{\beta} &= \frac{\sigma}{10} (f + \frac{1}{12} g_{;\lambda}^{\lambda}) \nu_{\beta} a^{\alpha\beta}, \\
q^{\alpha} \nu_{\alpha} &= \frac{5}{12} g^{\alpha} \nu_{\alpha}
\end{aligned} \tag{49}$$

The derivation of boundary conditions for a simply supported edge  $\partial_s$  is similar. Equations (48), (37), and (49) constitute the strong formulation of the problem.

#### 4.2. Discretization

The weak formulation (Eqs. (42), (44), (43), and (45)) involves covariant derivatives of various co- and contravariant vector and tensor components, complicating direct computation of residual forces and stiffness matrices. Therefore, unlike the first-order shear deformation theory for plates presented in [43], this refined shell theory employs a different approach. Leveraging the inherent smoothness of the weak formulation, Automatic Differentiation (AD) is used for symbolic representation. Specifically, the *Trilinos/Sacado* package provides the necessary AD capabilities.

The primal variables,  $u$ ,  $u_{\alpha}$ ,  $\psi_{\alpha}$ , and their corresponding variations  $\delta u$ ,  $\delta u_{\alpha}$ ,  $\delta \psi_{\alpha}$ , are assigned degrees of freedom (d.o.f.) with indices  $i_u$ ,  $i_{u_{\alpha}}$ ,  $i_{\psi_{\alpha}}$ ,  $i_{\delta u}$ ,  $i_{\delta u_{\alpha}}$ , and  $i_{\delta \psi_{\alpha}}$ , respectively. Defining  $\delta J = \delta W^m + \delta W^b + \delta W^s - \delta \mathcal{A}_{\text{ext}}$  as the first variation of the energy functional, the residual force and stiffness matrix corresponding to primal d.o.f.  $\delta a$  and  $b$  ( $a, b = u, u_{\alpha}, \psi_{\alpha}$ ) are computed as:

$$r_{\delta a} = \frac{\partial (\delta W^m + \delta W^b + \delta W^s - \delta \mathcal{A}_{\text{ext}})}{\partial \delta a} = \delta J . dx (i_{\delta a}) \tag{50}$$

$$K_{\delta a, b} = \frac{\partial r_{\delta a}}{\partial b} = \frac{\partial (\delta W^m + \delta W^b + \delta W^s - \delta \mathcal{A}_{\text{ext}})}{\partial \delta a \partial b} = \delta J .dx (i_{\delta a}) .dx (i_b) \quad (51)$$

We note that, to compute the double derivatives in Eq. (51), the symbolic variables  $\delta a$  and  $b$  must be of type `Sacado::Fad::DFad<Sacado::Fad::DFad<double>>`.

#### 4.3. Isogeometric analysis

As mentioned at the end of Section 3, accurate determination of the true average normal displacement  $\tilde{u}$  and rotation angle  $\varphi_\alpha$  necessitates  $C^1$  continuity. Isogeometric analysis (IGA) is well-suited for shell geometry discretization for two primary reasons: (i) Higher-order continuity: IGA readily provides the required  $C^1$  continuity through the use of non-uniform rational B-splines (NURBS) shape functions, (ii) Geometric flexibility: Complex geometries can be accurately represented by multiple surface patches connected at interfaces, with continuity preserved using techniques like the bending strip method [44]. Furthermore, the order of the NURBS basis functions can be conveniently increased via *hpk*-refinement.

NURBS shape functions used in IGA read:

$$\mathbf{S}(\xi_1, \xi_2) = \sum_{i=1}^m \sum_{j=1}^n \frac{N_i^p(\xi_1) N_j^q(\xi_2)}{\sum_{k=1}^m \sum_{l=1}^n w_{kl} N_k^p(\xi_1) N_l^q(\xi_2)} \mathbf{P}_{ij}. \quad (52)$$

Here,  $N_i^p$  and  $N_j^q$  are univariate B-spline basis functions of order  $p$  and  $q$ , respectively, computed using the recursive Cox-de-Boor formula:

$$N_i^p(\xi) = \frac{\xi - \xi_i}{\xi_{i+p} - \xi_i} N_i^{p-1}(\xi) + \frac{\xi_{i+p+1} - \xi_i}{\xi_{i+p+1} - \xi_{i+1}} N_{i+1}^{p-1}(\xi), \quad N_i^0(\xi) = \begin{cases} 1 & \xi_i \leq \xi \leq \xi_{i+1} \\ 0 & \text{otherwise} \end{cases}. \quad (53)$$

$\{\mathbf{P}_{ij}\}_{0 \leq i \leq m, 0 \leq j \leq n}$  represents the control point grid, and  $\{w_{ij}\}_{0 \leq i \leq m, 0 \leq j \leq n}$  are the corresponding control weights. The Cox-de-Boor formula (Eq. (53)) requires a global knot vector. To maintain the local nature of finite elements and enable parallel computation during assembly, Bézier decomposition [45] is employed.

#### 4.4. Structure of the finite element code

The proposed FSDT shell element is implemented within the `PlateAndShellApplication` extension of the Kratos Multiphysics framework kernel [46]. The `IsogeometricPlateAndShellApplication` extension enables

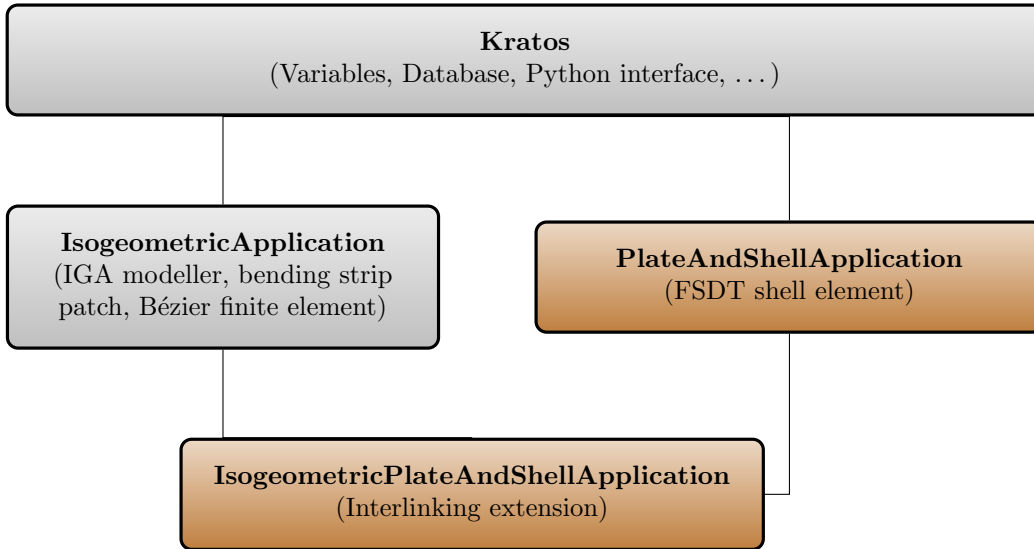


Figure 2: Structure of the computational code.

analysis using IGA. NURBS multipatch structures and Bézier elements are supported in the `IsogeometricApplication`. The relationships between these Kratos extensions are shown in Fig. 2.

## 5. Numerical examples

### 5.1. Semi-cylindrical shell under internal pressure with freely sliding side edges

We analyze a semi-cylindrical shell occupying the region defined by

$$0 \leq x \leq L, \quad 0 \leq \theta \leq \pi, \quad R - h/2 \leq r \leq R + h/2 \quad (54)$$

in cylindrical coordinates  $\{x, \theta, r\}$  (see Fig. 3). The shell is subjected to internal pressure  $p$  applied to its inner surface at  $r = R - h/2$ . For the 2D shell theory, we introduce rescaled surface coordinates  $\bar{x}^1 = x/h$  varying from 0 to  $\bar{L} = L/h$  and  $\bar{x}^2 = R\theta/h$  varying from 0 to  $\bar{W} = \pi R/h$ , where  $W = \pi R$  is the semi-circular circumference. For brevity, we drop the overbars on rescaled coordinates and quantities in the following theoretical development.

The middle surface in rescaled coordinates is described by:

$$\mathbf{z} = -x^1 \mathbf{e}_1 + R \cos \frac{x^2}{R} \mathbf{e}_2 + R \sin \frac{x^2}{R} \mathbf{e}_3. \quad (55)$$

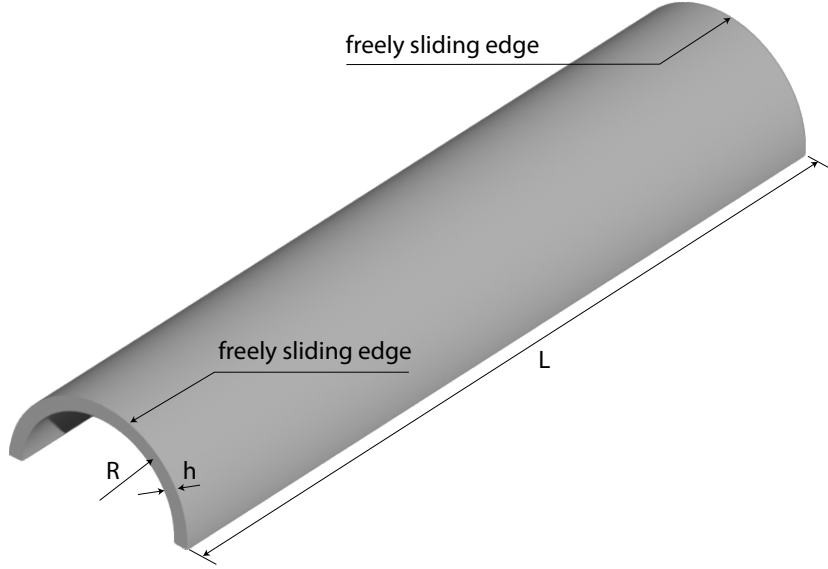


Figure 3: Schematic diagram of the semi-cylindrical shell

The tangent vectors to the coordinate lines on the middle surface are:

$$\mathbf{t}_1 = \mathbf{z}_{,1} = -\mathbf{e}_1, \quad \mathbf{t}_2 = \mathbf{z}_{,2} = -\sin \frac{x^2}{R} \mathbf{e}_2 + \cos \frac{x^2}{R} \mathbf{e}_3. \quad (56)$$

The unit normal vector is:

$$\mathbf{n} = \frac{\mathbf{t}_1 \times \mathbf{t}_2}{|\mathbf{t}_1 \times \mathbf{t}_2|} = \cos \frac{x^2}{R} \mathbf{e}_2 + \sin \frac{x^2}{R} \mathbf{e}_3. \quad (57)$$

In the 2D curvilinear coordinate system  $\{x^1, x^2\}$ , the components of the 2D metric tensor are  $\delta_{\alpha\beta}$ , the Kronecker delta. Consequently, the Christoffel symbols vanish, and covariant derivatives coincide with partial derivatives. Raising or lowering indices does not change tensor and vector components, so we represent them in covariant form with lower indices. The non-zero component of the second fundamental form is:

$$b_{11} = 0, \quad b_{12} = 0, \quad b_{22} = -\frac{1}{R}. \quad (58)$$

The mean curvature and  $b'_{\alpha\beta}$  are:

$$H = -\frac{1}{2R}, \quad b'_{11} = \frac{1}{2R}, \quad b'_{12} = 0, \quad b'_{22} = -\frac{1}{2R}. \quad (59)$$



Using Eq. (28), the extension and bending measures, and the rotation angles due to shear deformation are:

$$\begin{aligned}
\gamma_{11} &= u_{1,1}, & \gamma_{12} = \gamma_{21} &= \frac{1}{2}(u_{1,2} + u_{2,1}), & \gamma_{22} &= u_{2,2} + \frac{u}{R}, \\
\rho_{11} &= -\psi_{1,1}, & \rho_{22} &= -\psi_{2,2}, \\
\rho_{12} = \rho_{21} &= -\frac{1}{2}(\psi_{1,2} + \psi_{2,1}) + \frac{1}{4R}(u_{1,2} - u_{2,1}), \\
\varphi_1 &= u_{,1} + \psi_1, & \varphi_2 &= u_{,2} - \frac{u_2}{R} + \psi_2.
\end{aligned} \tag{60}$$

The energy density contributions (with overbars dropped) are:

$$\begin{aligned}
\Phi_{\text{cl}} &= \sigma(u_{1,1} + u_{2,2} + \frac{u}{R})^2 + (u_{1,1})^2 + (u_{2,2} + \frac{u}{R})^2 + \frac{1}{2}(u_{1,2} + u_{2,1})^2 \\
&+ \frac{1}{12} \left[ \sigma(\psi_{1,1} + \psi_{2,2})^2 + (\psi_{1,1})^2 + (\psi_{2,2})^2 \right. \\
&\left. + \frac{1}{2} \left( -\psi_{1,2} - \psi_{2,1} + \frac{1}{2R}(u_{1,2} - u_{2,1}) \right)^2 \right],
\end{aligned} \tag{61}$$

$$\begin{aligned}
\Phi_{\text{gc}} &= \frac{1}{6R} \left[ \left( \sigma \left( \frac{6}{5} \sigma - 1 \right) - 1 \right) \rho_{11} \gamma_{11} + (1 + \sigma) \left( 1 + \frac{6}{5} \sigma \right) \rho_{22} \gamma_{22} \right. \\
&\left. + \sigma \left( 1 + \frac{6}{5} \sigma \right) \rho_{22} \gamma_{11} + \sigma \left( \frac{1}{5} + \frac{6}{5} \sigma \right) \rho_{11} \gamma_{22} \right],
\end{aligned} \tag{62}$$

$$\Phi_{\text{sc}} = \frac{5}{12} \left[ (u_{,1} + \psi_1)^2 + \left( u_{,2} - \frac{u_2}{R} + \psi_2 \right)^2 \right]. \tag{63}$$

With pressure acting on the inner face,

$$f = p, \quad g = -p, \quad f_\alpha = g_\alpha = 0, \tag{64}$$

and the external work is:

$$\mathcal{A}_{\text{ext}} = \int_{\mathcal{S}} \left[ p \left( 1 - \frac{1}{2R} \right) u + \frac{\sigma}{2} p (u_{1,1} + u_{2,2} + \frac{u}{R}) + \frac{\sigma}{10} p (\psi_{1,1} + \psi_{2,2}) \right] d\omega. \tag{65}$$

We seek analytical solutions as benchmark solutions to validate our finite element implementation of 2D problems. For this purpose, we assume frictionless sliding of the side edges between rigid planes at  $x_1 = 0$  and  $x_1 = L$ . This implies the following boundary conditions:

$$u_1 = \psi_1 = 0, \quad u_2, u, \psi_2 \text{-arbitrary at } x_1 = 0, L. \tag{66}$$

For the bottom edges of the shell, located at  $x_2 = 0, W$ , we consider three boundary condition cases:

1. Freely sliding edges:

$$u_1 = u_2 = 0, \quad u \text{-arbitrary}, \quad \psi_1 = \psi_2 = 0 \quad \text{at } x_2 = 0, W. \quad (67)$$

2. Clamped edges:

$$u_1 = u_2 = u = \psi_1 = \psi_2 = 0 \quad \text{at } x_2 = 0, W. \quad (68)$$

3. Simply supported edges:

$$u_1 = u_2 = u = \psi_1 = 0, \quad \psi_2 \text{-arbitrary at } x_2 = 0, W. \quad (69)$$

These boundary conditions lead to a state of plane strain, where:

$$u_1 \equiv \psi_1 \equiv 0, \quad u_2, u, \psi_2 \text{ are function of } x_2 \text{ only.} \quad (70)$$

Consequently, Eq. (60) simplifies to:

$$\begin{aligned} \gamma_{11} &= 0, & \gamma_{12} &= 0, & \gamma_{22} &\equiv \gamma = u_{2,2} + \frac{1}{R}u, \\ \rho_{11} &= 0, & \rho_{12} &= 0, & \rho_{22} &\equiv \rho = -\psi_{2,2}, \\ \varphi_1 &= 0, & \varphi_2 &\equiv \varphi = u_{,2} - \frac{1}{R}u_2 + \psi_2, \end{aligned} \quad (71)$$

where the comma before the index 2 denotes the ordinary derivative with respect to  $x_2$ . The minimization problem (Eq. (34)) reduces to a 1-D problem (arc-like model, 1D-RST): Minimize

$$\begin{aligned} J &= \int_0^W \left[ (1+\sigma)(u_{2,2} + \frac{1}{R}u)^2 + \frac{1+\sigma}{12}(\psi_{2,2})^2 - \frac{1}{6}(1+\sigma)(1 + \frac{6}{5}\sigma)\frac{1}{R}(u_{2,2} + \frac{1}{R}u)\psi_{2,2} \right. \\ &\quad \left. + \frac{5}{12}(u_{,2} - \frac{1}{R}u_2 + \psi_2)^2 - p(1 - \frac{1}{2R})u - \frac{\sigma}{2}p(u_{2,2} + \frac{1}{R}u) - \frac{\sigma}{10}p\psi_{2,2} \right] dx_2 \end{aligned} \quad (72)$$

with respect to  $u_2, u, \psi_2$  subject to the kinematic boundary conditions. The integration over  $x_1$  yields a constant factor  $L$ , which is omitted in Eq. (72).

The Euler-Lagrange equations, obtained from the vanishing first variation of functional (72), are:

$$\begin{aligned} -n_{,2} - \frac{1}{R}q &= 0, \\ m_{,2} + q &= 0, \\ -q_{,2} + \frac{1}{R}n &= p(1 - \frac{1-\sigma}{2R}), \end{aligned} \quad (73)$$

where

$$\begin{aligned}
n &= \frac{\partial\Phi}{\partial\gamma} = 2(1+\sigma)\gamma + \frac{1}{6}(1+\sigma)\left(1 + \frac{6}{5}\sigma\right)\frac{1}{R}\rho, \\
m &= \frac{\partial\Phi}{\partial\rho} = \frac{1}{6}(1+\sigma)\rho + \frac{1}{6}(1+\sigma)\left(1 + \frac{6}{5}\sigma\right)\frac{1}{R}\gamma, \\
q &= \frac{\partial\Phi}{\partial\varphi} = \frac{5}{6}\varphi.
\end{aligned} \tag{74}$$

Substituting Eq. (74) with  $\gamma, \rho, \varphi$  from Eq. (71) into Eq. (73) yields three second-order ordinary differential equations for  $u_2, \psi_2, u$ .

For comparison, we also analyze the shell using Sanders-Koiter classical shell theory (CST). Assuming plane strain, the problem reduces to minimizing the 1-D functional (1D-CST)

$$J_{\text{cl}} = \int_0^W \left[ (1+\sigma)(u_{2,2} + \frac{1}{R}u)^2 + \frac{1+\sigma}{12}(u_{,22} - \frac{1}{R}u_{2,2})^2 - pu \right] dx_2 \tag{75}$$

with respect to  $u_2$  and  $u$  subject to the kinematic boundary conditions. The Euler-Lagrange equations are:

$$\begin{aligned}
-n_{,2} - \frac{1}{R}m_{,2} &= 0, \\
m_{,22} + \frac{1}{R}n &= p,
\end{aligned} \tag{76}$$

where

$$\begin{aligned}
n &= 2(1+\sigma)\gamma, & \gamma &= u_{2,2} + \frac{1}{R}u, \\
m &= \frac{1}{6}(1+\sigma)\rho, & \rho &= u_{,22} - \frac{1}{R}u_{2,2}.
\end{aligned} \tag{77}$$

For Case 1 (Eq. (67)), the boundary conditions derived from the vanishing first variation of  $J$  and the arbitrariness of  $u$  at  $x_2 = 0, W$  are:

$$u_2 = \psi_2 = 0, \quad q = 0 \quad \text{at } x_2 = 0, W. \tag{78}$$

The solution is

$$u = \frac{pR^2}{2(1+\sigma)}\left(1 - \frac{1-\sigma}{2R}\right), \quad u_2 = \psi_2 = 0, \tag{79}$$

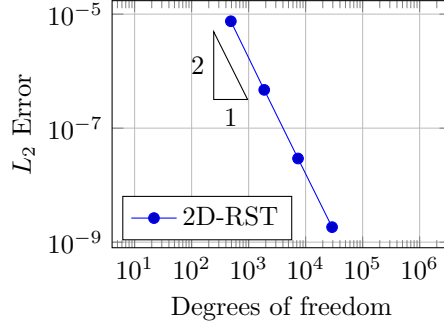


Figure 4: Convergence of 2D-RST displacement in the first case against the analytical solution of 1D-RST in terms of  $L_2$  error.

yielding

$$\gamma = \frac{pR}{2(1+\sigma)} \left(1 - \frac{1-\sigma}{2R}\right), \quad \rho = \varphi = 0. \quad (80)$$

This solution satisfies Eqs. (73), (74), and the boundary conditions (Eq. (69)). This problem has a known 3D elasticity solution. The radial displacement is [47]:

$$w_r = \frac{pR^2}{4} \left(1 - \frac{1}{2R}\right)^2 \left[ (1-2\nu)(1+\zeta) + \left(1 + \frac{1}{2R}\right)^2 \frac{1}{1+\zeta} \right], \quad (81)$$

where  $\zeta = \xi/R$  and  $\zeta \in (-1/(2R), 1/(2R))$ . The average displacement from Eq. (81) agrees with Eq. (79) up to  $h/R$ . Figure 4 shows the  $L_2$  error convergence of the 2D-RST displacement compared to Eq. (79). Classical shell theory (CST) [3, 4], while accurate for stress resultants and bending moments, exhibits large displacement errors. The 1D-CST solution (Eqs. (75)-(77)) for mean displacements is

$$\begin{aligned} u &= -\frac{1}{2}pR^2(1-\nu) \left( \frac{\pi}{2} \sin(x_2/R) - 2 \right), \\ u_2 &= \frac{1}{2}pR^2(1-\nu) \left( \frac{\pi}{2} - \frac{\pi}{2} \cos(x_2/R) - x_2/R \right), \end{aligned} \quad (82)$$

which results in a 100% error compared to Eqs. (79) and (81). This discrepancy highlights the limitations of classical shell theory in accurately predicting displacements, as explained in [5].

For Case 2 with clamped bottom edges, an analytical solution of 1D-RST can be found in terms of exponential functions involving the roots of a cubic

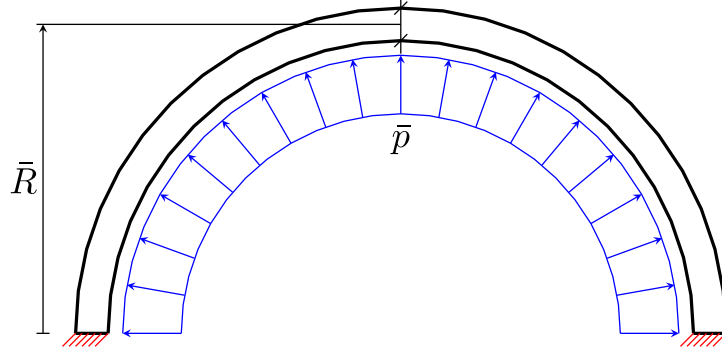


Figure 5: Schematic diagram of the half-ring of thickness 1 and radius  $\bar{R}$  under internal pressure  $\bar{p}$ .

polynomial equation. However, this solution is quite cumbersome. Therefore, we opt for a numerical approach. We first rewrite Eq. (71) as:

$$\begin{aligned} u_{2,2} &= \gamma - \frac{1}{R}u, \\ \psi_{2,2} &= -\rho, \\ u_{,2} &= \varphi + \frac{1}{R}u_2 - \psi_2, \end{aligned} \quad (83)$$

Next, we eliminate  $\rho$  from Eqs. (74)<sub>1</sub> and (74)<sub>2</sub> to express  $\gamma$  in terms of  $n$  and  $m$ . Differentiating and using Eqs. (73)<sub>1</sub> and (73)<sub>2</sub>, we obtain:

$$\gamma_{,2} = \frac{\sigma}{2(1+\sigma)R[1 - \frac{1}{12}(1 + \frac{6}{5}\sigma)^2 \frac{1}{R^2}]} \varphi. \quad (84)$$

Similarly, eliminating  $\gamma$  from Eqs. (74)<sub>1</sub> and (74)<sub>2</sub>, expressing  $\rho$  in terms of  $n$  and  $m$ , differentiating, and using Eqs. (73)<sub>1</sub> and (73)<sub>2</sub>, we get:

$$\rho_{,2} = -\frac{5(1 - \frac{1}{12}(1 + \frac{6}{5}\sigma) \frac{1}{R^2})}{(1+\sigma)[1 - \frac{1}{12}(1 + \frac{6}{5}\sigma)^2 \frac{1}{R^2}]} \varphi. \quad (85)$$

Finally, from Eqs. (73)<sub>3</sub> and (74)<sub>3</sub>, we have:

$$\varphi_{,2} = \frac{6}{5} [2(1+\sigma) \frac{1}{R} \gamma + \frac{1}{6}(1+\sigma)(1 + \frac{6}{5}\sigma) \frac{1}{R^2} \rho - p(1 - \frac{1-\sigma}{2R})]. \quad (86)$$

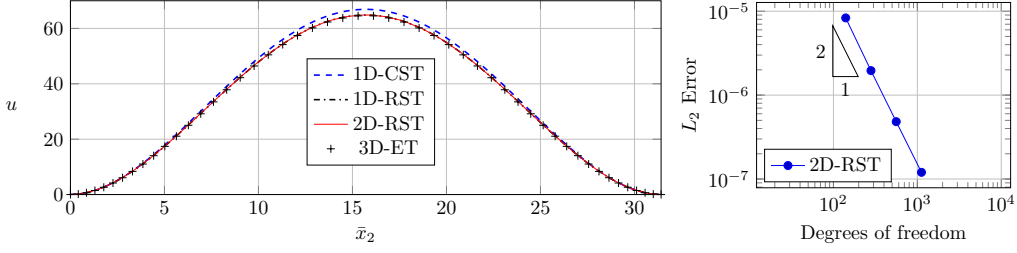


Figure 6: Normal displacement  $\bar{u}$  of a semi-cylindrical shell under external pressure with freely sliding side edges and clamped bottom edges (second case) as function of the rescaled circumferential coordinate  $\bar{x}_2 = \pi \bar{R} \theta$  ( $\bar{R} = 10$ ).

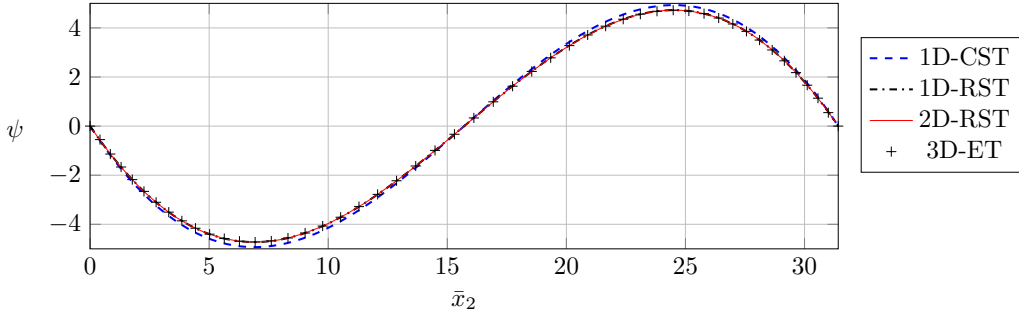


Figure 7: Rescaled rotation angle  $\bar{\psi}_2$  of a semi-cylindrical shell under external pressure with freely sliding side edges and clamped bottom edges (second case) as function of the rescaled circumferential coordinate  $\bar{x}_2 = \pi \bar{R} \theta$  ( $\bar{R} = 10$ ).

Introducing  $v = u_{,2}$  and  $\vartheta = \rho_{,2}$ , the 1D-CST system (Eqs. (76) and (77)) becomes:

$$\begin{aligned}
 u_{,2} &= v, \\
 u_{2,2} &= \gamma - \frac{1}{R}u, \\
 \gamma_{,2} &= \frac{1}{12R}\vartheta, \\
 v_{,2} &= \rho + \frac{1}{R}\left(\gamma - \frac{1}{R}u\right), \\
 \rho_{,2} &= \vartheta, \\
 \vartheta_{,2} &= \frac{6}{1+\sigma}p - \frac{12}{R}\gamma.
 \end{aligned} \tag{87}$$

Equations (83) and (84)-(86) form a system of six first-order ODEs for

$u_2, \psi_2, u, \gamma, \rho, \varphi$ , subject to the boundary conditions:

$$u_2 = \psi_2 = u = 0 \quad \text{at } x_2 = 0, W. \quad (88)$$

For 1D-CST, we have six first-order ODEs (Eq. (87)) for  $u, u_2, \gamma, v, \rho, \vartheta$ , subject to:

$$u = u_2 = v = 0 \quad \text{at } x_2 = 0, W. \quad (89)$$

These two-point boundary-value problems are solved using Matlab's `bvp4c` function.

To demonstrate the asymptotic accuracy of our FE-implementation of 2D-RST, we also compare its numerical solution with that of 3D elasticity theory (3D-ET). In this case, under plane strain conditions, the rescaled problem reduces to the two-dimensional analysis of a half-ring having thickness 1 (see Fig. 5), which can be solved using 2D isogeometrical analysis (IGA) with solid elements. After solving this 2D problem, the mean radial displacement and rotation angle over the shell's thickness are evaluated in accordance with Eq. (39).

Both the shell analysis and the elastic solid analysis employ cubic-order NURBS discretization with sufficiently fine meshes. Using overbars to denote rescaled quantities, we present the results of numerical simulation below. In all numerical simulations, we set  $\nu = 0.3$  and  $\bar{p} = 1$ , so that the solution is normalized. Due to linearity, the solution for any real  $\bar{p}$  can be obtained by multiplying the normalized solution by  $\bar{p}$ .

Fig. 6 shows, on the right, the convergence rate of the 2D-RST solution to that of the 1D-RST for the thin shell with  $\bar{R} = 10$ , demonstrating that our FE-implementation is free from membrane and shear locking. It also plots, on the left, the normal mean displacement  $\bar{u}$  versus  $\bar{x}_2$  computed using all four theories (1D-CST, 1D-RST, 2D-RST, 3D-ET). The 2D-RST solution (red line) matches that of 1D-RST (black dotted-dashed line) perfectly. Since the shell is thin, this 2D-RST solution agrees quite well with that of 3D-ET (black plus points). The 1D-CST solution deviates noticeably from the others. Fig. 7 shows the plot of the rescaled rotation angle  $\bar{\psi}_2$  versus  $\bar{x}_2$  computed using all four theories. For classical shell theory, the rotation angle  $\bar{\psi}_2$  is due to bending only and is computed as  $\bar{\psi}_2 = -\bar{u}_{,22} + \bar{u}_{2,2}/\bar{R}$ . We observe a perfect match between the 2D-RST and 1D-RST solutions, and an almost perfect match between them and the 3D-ET solution. Here too, the 1D-CST solution deviates noticeably from the others.

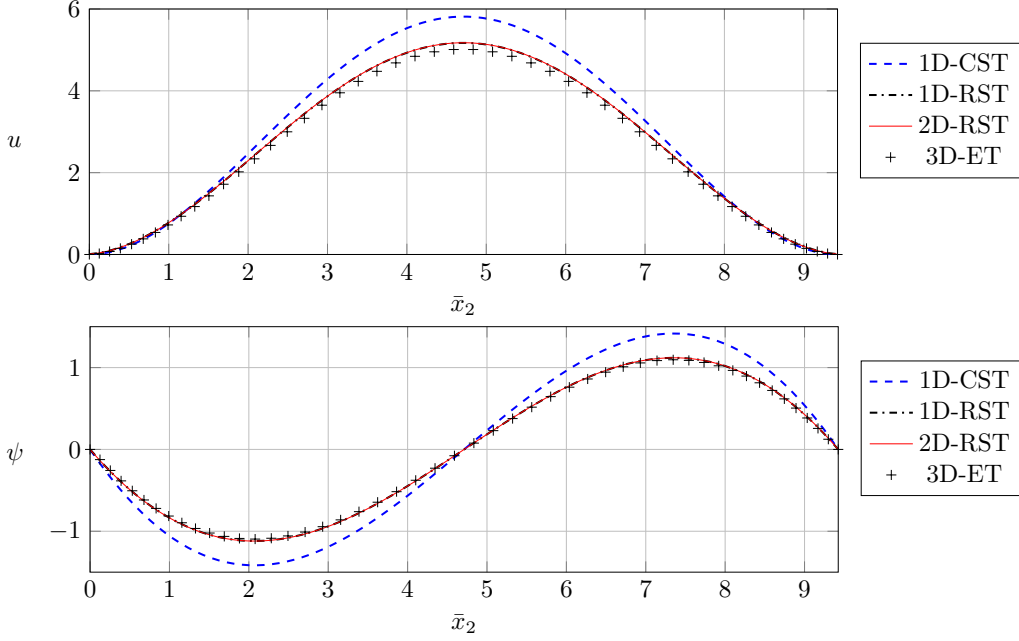


Figure 8: Normal displacement  $\bar{u}$  and rescaled rotation angle  $\bar{\psi}_2$  of a semi-cylindrical shell under external pressure with freely sliding side edges and clamped bottom edges (second case) as function of the rescaled circumferential coordinate  $\bar{x}_2 = \pi \bar{R} \theta$  ( $\bar{R} = 3$ ).

We now check whether 2D-RST is applicable to moderately thick shells. For this purpose, we set  $\bar{R} = 3$ , while keeping all other parameters unchanged. The plots of the mean normal displacement  $\bar{u}$  and rescaled rotation angle  $\bar{\psi}_2$  ( $-\bar{u}_{,\bar{x}_2} + \bar{u}_{\bar{x}_2,2}/\bar{R}$  for CST) as functions of  $\bar{x}_2$  are shown in Fig. 8 for  $\nu = 0.3$ ,  $\bar{R} = 3$ , and  $\bar{p} = 1$ . The curves for 1D-RST and 2D-RST, which match each other perfectly, agree well with that of 3D-ET, showing that 2D-RST is applicable also to moderately thick shells. The classical shell theory shows a large deviation from 3D-ET, indicating that CST can no longer be used for moderately thick shells.

For Case 3 with simply supported bottom edges, the equations remain the same, but the boundary conditions become:

$$u_2 = u = 0, \quad m = -\frac{\sigma}{10} p \quad \text{at } x_2 = 0, W. \quad (90)$$

The conditions  $m = -\frac{\sigma}{10} p$  at  $x_2 = 0, W$  arise from the vanishing first variation of functional (72) and the arbitrariness of  $\psi_2$  at  $x_2 = 0, W$ . For 1D-CST, the



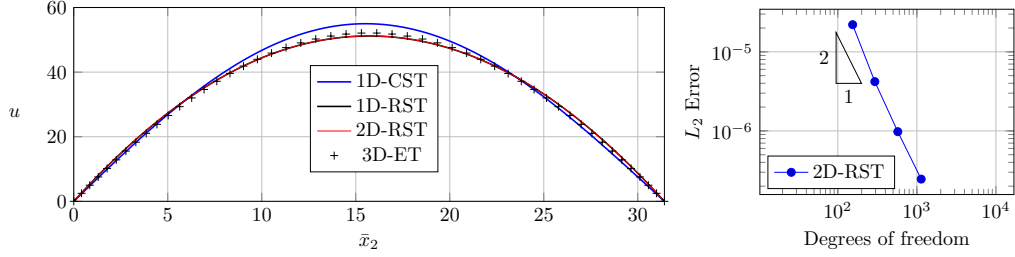


Figure 9: Normal displacement  $\bar{u}$  of a semi-cylindrical shell under external pressure with freely sliding side edges and simply-supported bottom edges (third case) as function of the rescaled circumferential coordinate  $\bar{x}_2 = \pi \bar{R} \theta$  ( $\bar{R} = 10$ ).

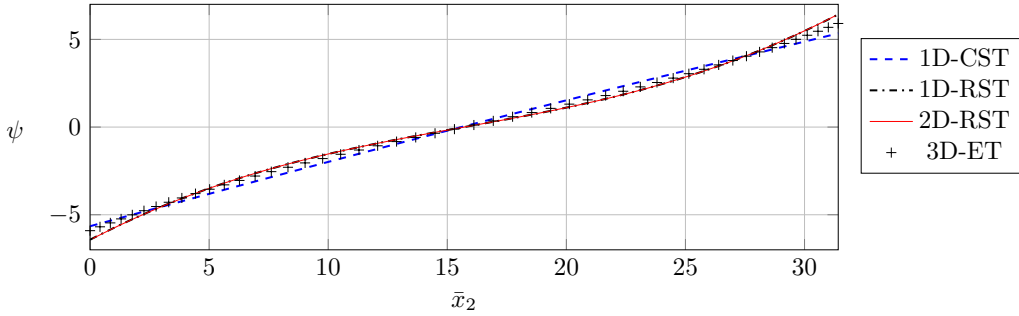


Figure 10: Rescaled rotation angle  $\bar{\psi}_2$  of a semi-cylindrical shell under external pressure with freely sliding side edges and simply-supported bottom edges (third case) as function of the rescaled circumferential coordinate  $\bar{x}_2 = \pi \bar{R} \theta$  ( $\bar{R} = 10$ ).

boundary conditions are:

$$u = u_2 = \vartheta = 0 \quad \text{at } x_2 = 0, W. \quad (91)$$

These two-point boundary-value problems are solved using Matlab's `bvp4c` function. Concerning the boundary conditions within 3D-ET: Since exact boundary conditions within 3D-ET for the simply supported edge are absent, we propose boundary conditions that best mimic those of the 2D shell theory. As such, we impose the following constraints: under the plane strain conditions, the mean displacements must vanish:

$$\langle w_2 \rangle = 0, \quad \langle w \rangle = 0. \quad (92)$$

Another condition, namely that the rotation  $\psi_2$  is not constrained, cannot be directly imposed within 3D-ET. However, its consequence,  $m = -\frac{\sigma}{10}p$ , can

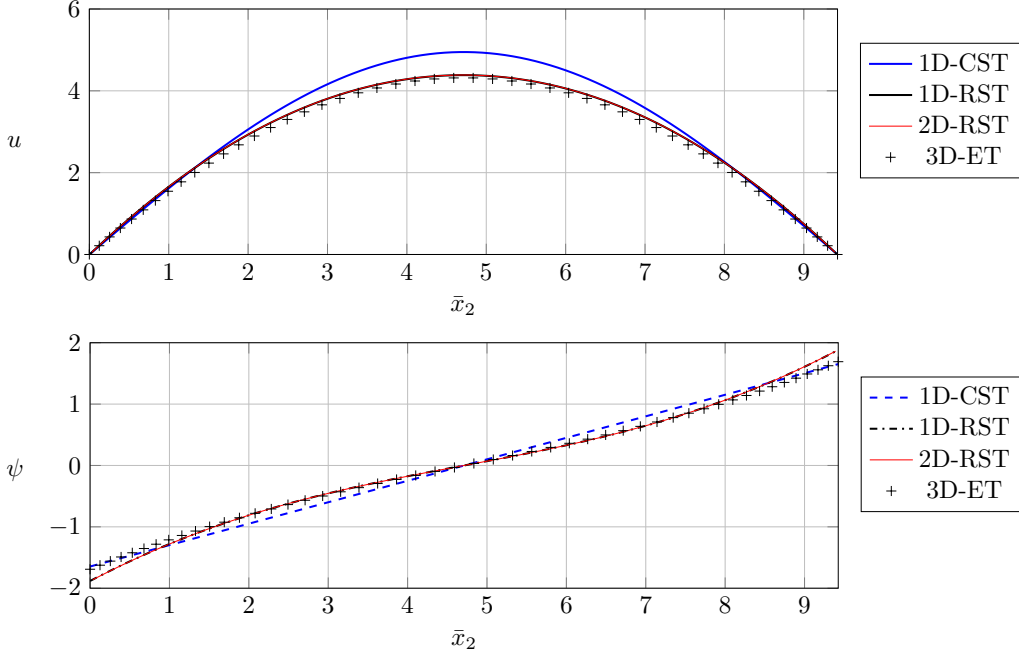


Figure 11: Normal displacement  $\bar{u}$  and rescaled rotation angle  $\bar{\psi}_2$  of a semi-cylindrical shell under external pressure with free side edges and simply-supported bottom edges (third case) as function of the rescaled circumferential coordinate  $\bar{x}_2 = \pi\bar{R}\theta$  ( $\bar{R} = 3$ ).

be imposed by specifying at the bottom edges the traction that gives such a bending moment, namely:

$$\sigma_{22}(\bar{r}, \theta) = -\frac{6\sigma}{5}\bar{p}(\bar{r} - \bar{R}) \quad \text{at } \theta = 0, \pi. \quad (93)$$

After solving the plane strain problem for the half-ring, the mean radial displacement and rotation angle over the shell's thickness are evaluated in accordance with Eq. (39), as in the previous case.

The mean normal displacement  $\bar{u}$  and rescaled rotation angle  $\bar{\psi}_2$  ( $-\bar{u}_{,\bar{2}\bar{2}} + \bar{u}_{\bar{2},\bar{2}}/\bar{R}$  for CST) as functions of  $\bar{x}^2$  are shown in Fig. 9 (left) and Fig. 10, respectively, for  $\nu = 0.3$ ,  $\bar{R} = 10$ , and  $p = 1$ . In Fig. 9 (right) we show also the convergence rate of the 2D-RST solution to that of the 1D-RST. We observe again the perfect match between 2D-RST and 1D-RST, and the almost perfect match between them and 3D-ET. The CST differs from them noticeably.

If we set  $\bar{R} = 3$  (moderately thick shell) while keeping all other param-

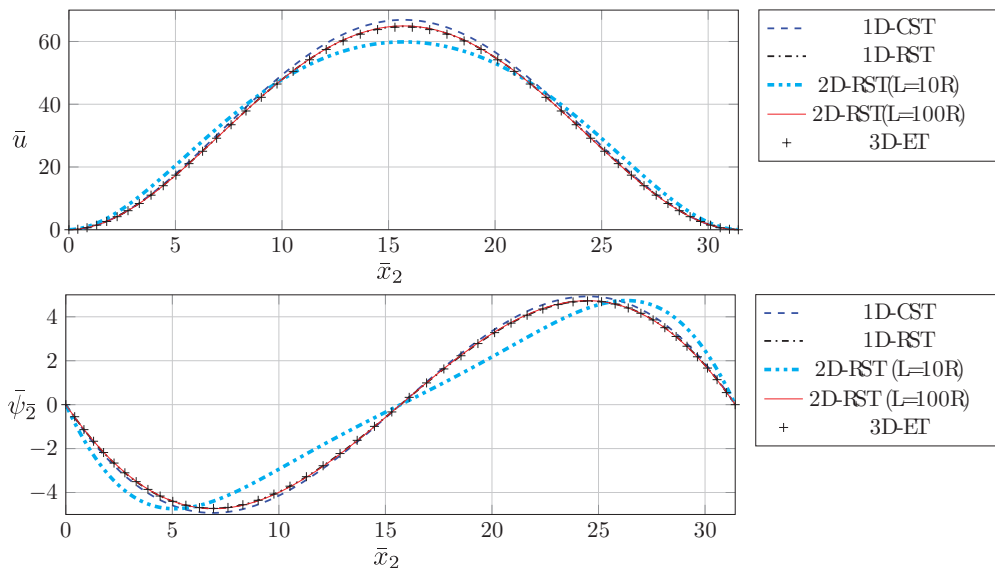


Figure 12: Normal displacement  $\bar{u}$  and rescaled rotation angle  $\bar{\psi}_2$  of a semi-cylindrical shell under external pressure with free side edges and clamped bottom edges (second case) as function of the rescaled circumferential coordinate  $\bar{x}_2 = \pi \bar{R} \theta$  ( $\bar{R} = 10$ ).

ters unchanged, we see that 2D-RST and 1D-RST still agree well with 3D-ET (see Fig. 11, which plots  $\bar{u}$  and  $\bar{\psi}_2$  computed according to all four theories). However, CST deviates considerably from the others. This comparison confirms the applicability of 2D-RST for moderately thick shells, but also shows that 2D-CST can no longer be used.

### 5.2. Semi-cylindrical shell under internal pressure with free side edges

This subsection investigates the behavior of a semi-cylindrical shell subjected to internal pressure, focusing on the impact of free side edges and varying bottom edge constraints. We analyze the normal displacement  $\bar{u}$  and rotation angle  $\bar{\psi}_2$  along the circumferential coordinate, leveraging reduced 1-D models and comparisons with 2D-RST solution in the mid-cross-section and plane strain ET solution.

For long cylindrical shells with free side edges, where  $L \gg R \gg h$ , the 1-D models provide accurate benchmark solutions at the shell's mid-cross-section. This is due to the negligible influence of the free side edge boundary effects in the central region, resulting in almost translational invariance along the  $x_1$ -direction. Consequently, a plane strain state can be assumed there,

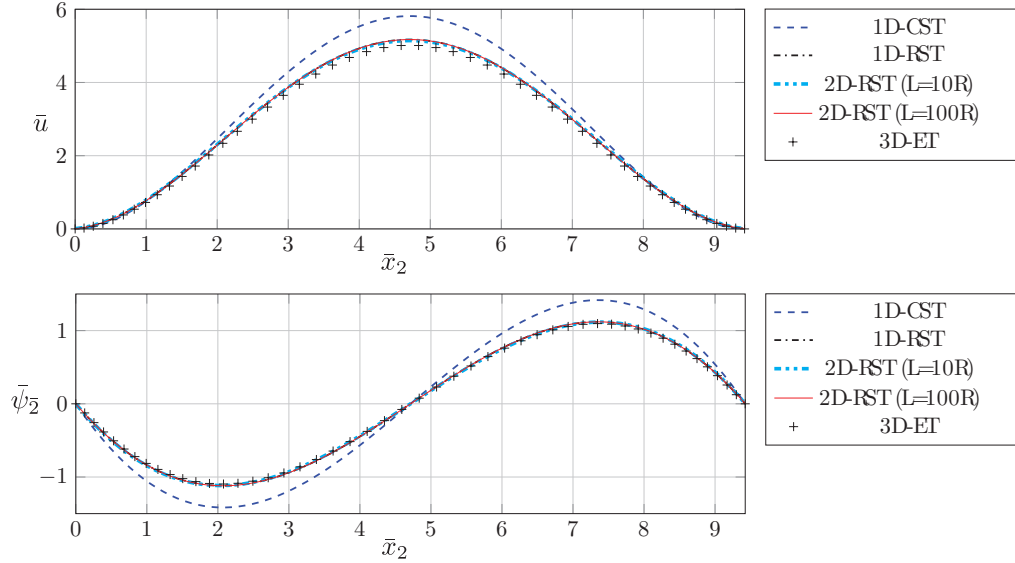


Figure 13: Normal displacement  $\bar{u}$  and rescaled rotation angle  $\bar{\psi}_2$  of a semi-cylindrical shell under external pressure with free side edges and clamped bottom edges (second case) as function of the rescaled circumferential coordinate  $\bar{x}_2 = \pi\bar{R}\theta$  ( $\bar{R} = 3$ ).

enabling the application of the arc-like model (1D-RST). Similarly, the 3D-ET simplifies to a 2D problem for the half-ring in the shell's central portion.

Figure 12 illustrates the mean normal displacement  $\bar{u}$  and rescaled rotation angle  $\bar{\psi}_2$  as functions of the rescaled circumferential coordinate  $\bar{x}_2 = \pi\bar{R}\theta$ , calculated using the 2D-RST at the mid-section ( $\bar{x}_1 = \bar{L}/2$ ) for clamped bottom edges. Comparisons are made with 1D-CST, 1D-RST, and plane strain ET solutions. By varying  $\bar{L}$  (setting it to  $10\bar{R}$  and  $100\bar{R}$ ) while maintaining  $\nu = 0.3$ ,  $\bar{R} = 10$ , and  $p = 1$ , we observe that the 2D-RST solution converges to the 1D-RST solution as  $\bar{L}$  increases, aligning closely with the 3D-ET results.

For moderately thick shells ( $\bar{R} = 3$ ) with clamped bottom edges, Figure 13 shows similar trends. The 2D-RST solutions at varying  $\bar{L}$  values confirm convergence to the 1D-RST solution. Comparisons with CST and ET demonstrate the continued applicability of RST, while highlighting the inadequacy of CST in this thickness regime.

We also examine semi-cylindrical shells with free side edges and simply supported bottom edges. As before, the free side edge effects are negligible in the central region for  $\bar{L} \gg \bar{R}$ . Numerical results presented in Figures 14 and

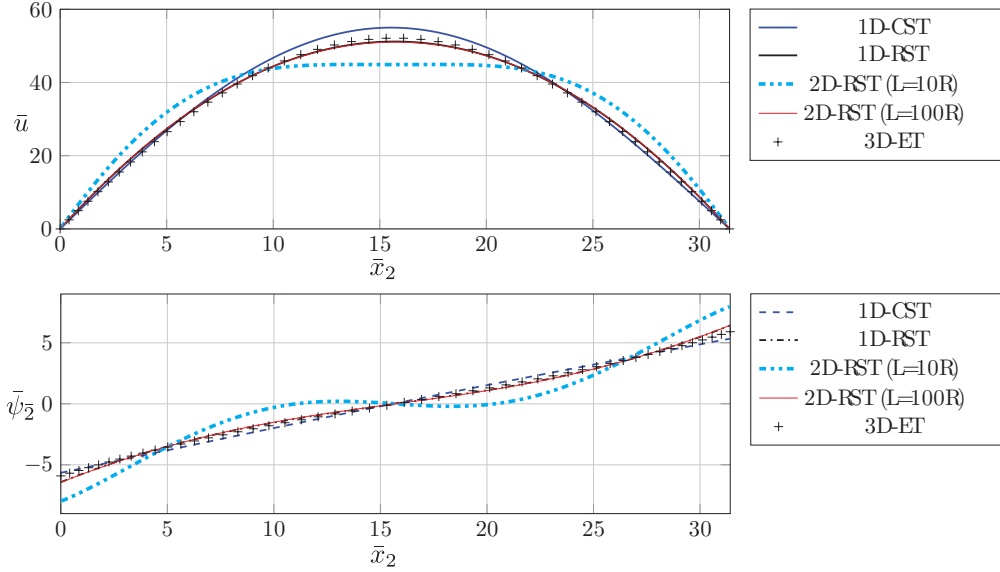


Figure 14: Normal displacement  $\bar{u}$  and rescaled rotation angle  $\bar{\psi}_2$  of a semi-cylindrical shell under external pressure with free side edges and simply-supported bottom edges (third case) as function of the rescaled circumferential coordinate  $\bar{x}_2 = \pi \bar{R} \theta$  ( $\bar{R} = 10$ ).

15 validate this observation. These figures further illustrate the 2D-RST's applicability to both thin and moderately thick shells, while reinforcing CST's limitations for moderately thick shells. Importantly, the FE implementation of the 2D-RST demonstrates both locking-free behavior and asymptotic accuracy across all numerical simulations.

### 5.3. A structure with two plates and a spherical cap under external pressure

To showcase the applicability of developed shell formulation in practical application, the deformation of a structure consisting of two orthogonal plates and a spherical cap subjected to external pressure, is investigated. The structure is defined within a Cartesian coordinate system  $(z_1, z_2, z_3)$ , with the  $(z_1, z_2)$ -plane coinciding with the base. The mid-surface of the first plate,  $\mathcal{P}_1$ , is described by:

$$\mathcal{P}_1 = \{(z_1, 0, z_3) \mid |z_1| \leq D, 0 \leq z_3 \leq c - \sqrt{R^2 - z_1^2}\}, \quad (94)$$

where  $c = H + \sqrt{R^2 - D^2}$  (see Figure 16). Note that the full width of  $\mathcal{P}_1$  extends to  $|z_1| \leq D + h/2$ , but due to  $h \ll D$ , we focus on the portion

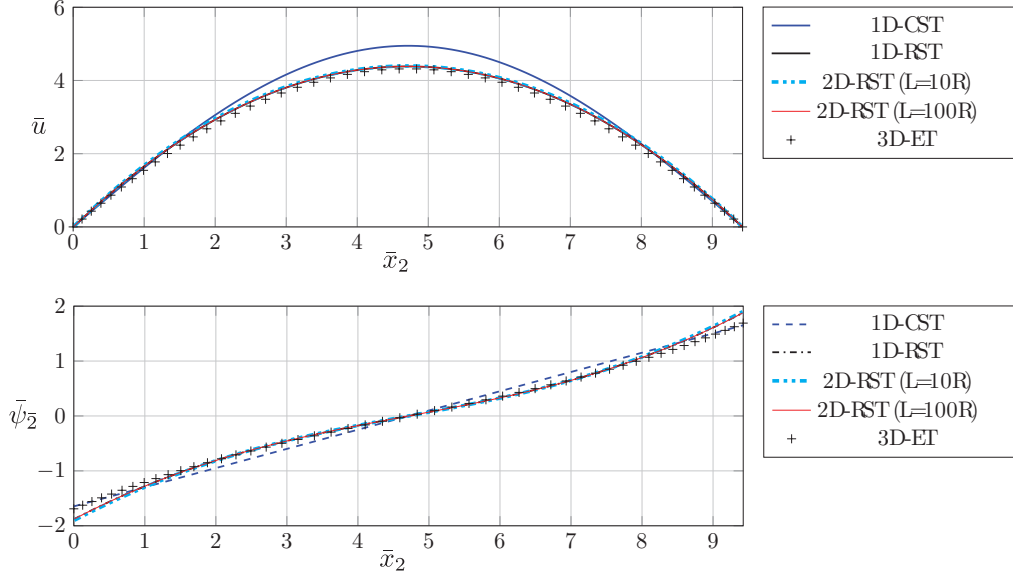


Figure 15: Normal displacement  $u$  and rotation  $\psi$  of a semi-cylindrical shell under external pressure with free side edges and simply-supported bottom edges (third case) as function of the rescaled circumferential coordinate  $\bar{x}_2 = \pi\bar{R}\theta$  ( $\bar{R} = 3$ ).

intersecting the mid-surface. Similarly, the mid-surface of the second plate,  $\mathcal{P}_2$ , is:

$$\mathcal{P}_2 = \{(0, z_2, z_3) \mid |z_2| \leq D, 0 \leq z_3 \leq c - \sqrt{R^2 - z_2^2}\}. \quad (95)$$

The spherical cap's mid-surface,  $\mathcal{P}_3$ , is:

$$\mathcal{P}_3 = \{(z_1, z_2, z_3) \mid z_1^2 + z_2^2 \leq D^2, z_3 = c - \sqrt{R^2 - z_1^2 - z_2^2}\}. \quad (96)$$

We define  $R\phi$  (azimuthal) and  $R\theta$  (polar) as the curvilinear coordinates on  $\mathcal{P}_3$ . All components are made of the same material, with a uniform thickness  $h$ , where  $h \ll D$ . The overall mid-surface of the structure is  $\mathcal{S} = \mathcal{P}_1 \cup \mathcal{P}_2 \cup \mathcal{P}_3$ . A constant pressure  $p$  is applied to the cap's top surface, while the plates' bottom edges are clamped. The remaining boundaries are traction-free.

The energy functional remains consistent with Eq. (11), with  $\Phi(\gamma_{\alpha\beta}, \rho_{\alpha\beta}, \varphi_\alpha)$  defined by Eqs. (12) and (13). The external work is given by:

$$\mathcal{A}_{\text{ext}} = \int_{\mathcal{P}_3} \left[ -p(1 + h/R)u + \frac{\sigma h}{2} p \gamma_\beta^\beta + \frac{1}{10} \sigma h^2 p \rho_\beta^\beta \right] d\omega. \quad (97)$$

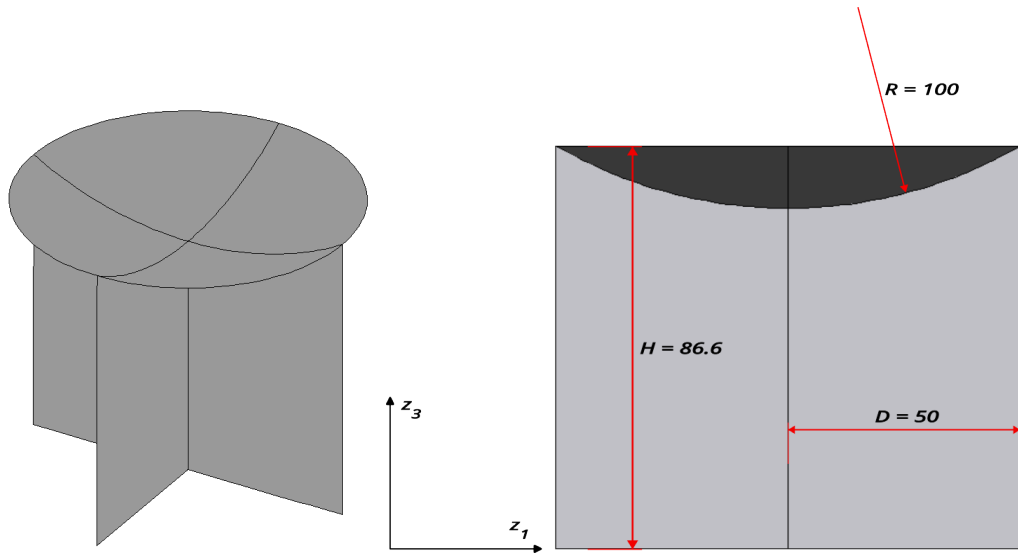


Figure 16: The spherical cap structure and its  $(z_1, z_3)$ -cross section. The unit of dimension is in cm.

The mid-surfaces  $\mathcal{P}_1$ ,  $\mathcal{P}_2$ , and  $\mathcal{P}_3$  intersect along three lines, where continuity of displacement and rotation vectors is enforced. Rotations about surface normals are constrained, considering only tangential components. At the triple point  $(0, 0, c - R)$ , where all surfaces meet, the rotation vector is zero.

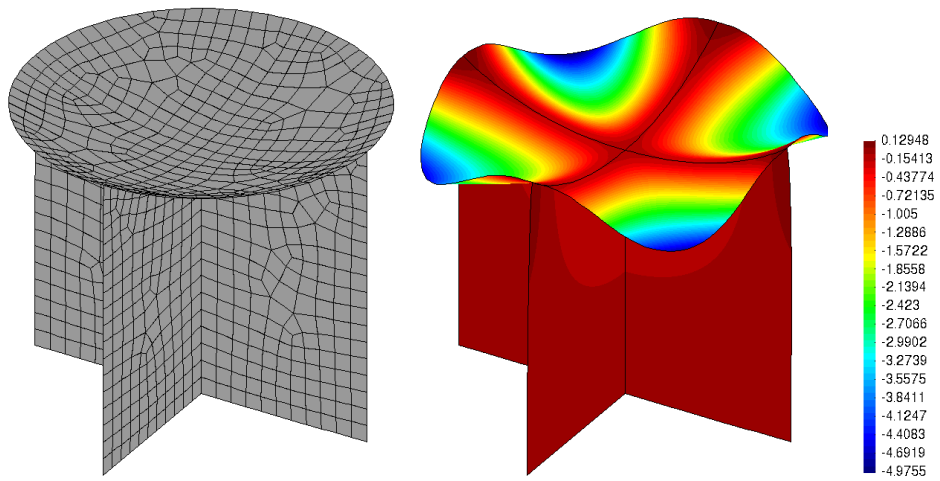


Figure 17: Mesh (left) and  $z_3$ -displacement of the spherical cap structure (right). The deformed structure is visualized with scale factor = 3.

The structure is discretized using 1082 Q9 elements with material properties:  $E = 2 \times 10^7$  N/cm<sup>2</sup>,  $\nu = 0.3$ , and  $h = 1$  cm. The applied pressure is  $p = 10^3$  N/cm<sup>2</sup>. Figure 17 depicts the deformed structure and its  $z_3$ -displacement. Figure 18 illustrates the rotation vector of the spherical cap projected onto  $\mathbf{t}_\phi$  (azimuthal) and  $\mathbf{t}_\theta$  (polar), showing that the azimuthal rotation vanishes along the intersections of the shell and plates.

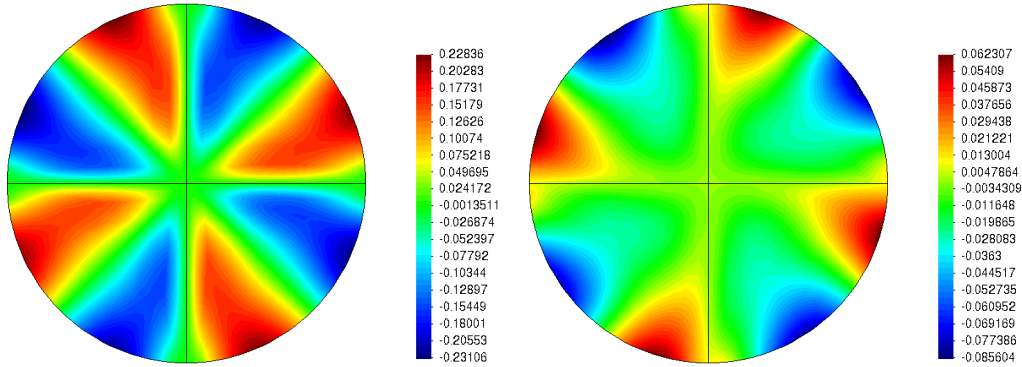


Figure 18: Rotation angle projected on  $\mathbf{t}_\phi$  (left) and  $\mathbf{t}_\theta$  (right) of the spherical cap structure.

## 6. Conclusion

This work presents a novel rescaled formulation of refined shell theory that is inherently free from membrane and shear locking. Combined with an isogeometric finite element implementation, this formulation achieves asymptotic accuracy in shell structure analysis. This combined achievement - asymptotic accuracy and freedom from locking - is key contributions of our paper. Unlike prior methods that often suggest numerical techniques to gain stability or accuracy, hence complicates the formulation further, our approach is mathematical based, concise and rigorous. This enables a straightforward implementation in the numerical code and yields an efficient pathway for analysis of shell structures, especially where accurate stress/displacement prediction in thin/moderately thick shells is crucial. Last but not least, our formulation still relies on the linear kinematics assumption. Future work will develop accurate and locking-free FE implementations for nonlinear refined shell theory, including applications to buckling analysis and shell theories for complex materials.



## References

- [1] A.L. Goldenveizer, Theory of elastic thin shells: solid and structural mechanics, vol. 2, Elsevier, 2014.
- [2] V.L. Berdichevsky, Variational Principles of Continuum Mechanics, Springer, 2009.
- [3] J.L. Sanders, An improved first-approximation theory for thin shells, NASA Tech. Rep., 1 (1959).
- [4] W.T. Koiter, A consistent first approximation in the general theory of thin elastic shells, in: Proceedings of the IUTAM Symposium on the Theory of Thin Elastic Shells, North-Holland Amsterdam, 1960, pp. 12–33.
- [5] V.L. Berdichevsky, V. Misyura, Effect of accuracy loss in classical shell theory, Journal of Applied Mechanics, 59 (2S) (1992) S217–S223.
- [6] V.L. Berdichevsky, Variational-asymptotic method of constructing a theory of shells, Journal of Applied Mathematics and Mechanics, 43 (4) (1979) 711–736.
- [7] V.L. Berdichevsky, Variational-asymptotic method of constructing the nonlinear shell theory, in: W.T. Koiter, G.K. Mikhailov (Eds.), Proceedings of IUTAM Symposium on Shell Theory, North-Holland, Amsterdam, 1979, pp. 137–161.
- [8] E. Reissner, The effect of transverse shear deformation on the bending of elastic plates, J. Appl. Mech., 12 (2) (1945) 69–77.
- [9] V.G. Sutyrin, Derivation of plate theory accounting asymptotically correct shear deformation, J. Appl. Mech., 64 (1997) 905–915.
- [10] W. Yu, Mathematical construction of a Reissner–Mindlin plate theory for composite laminates, International Journal of Solids and Structures, 42 (26) (2005) 6680–6699.
- [11] Z. Yifeng, C. Lei, W. Yu, Variational asymptotic modeling of the thermomechanical behavior of composite cylindrical shells, Composite Structures, 94 (3) (2012) 1023–1031.

- [12] Z. Yifeng, C. Lei, W. Yu, Variational asymptotic modeling of the multilayer functionally graded cylindrical shells, *Composite Structures*, 94 (3) (2012) 966–976.
- [13] R.G. Burela, D. Harursampath, Vam applied to dimensional reduction of non-linear hyperelastic plates, *International Journal of Engineering Science*, 59 (2012) 90–102.
- [14] R.G. Burela, D. Harursampath, Asymptotically-accurate nonlinear hyperelastic shell constitutive model using variational asymptotic method, in: H. Altenbach et al. (Eds.), *Recent Developments in the Theory of Shells*, Springer, 2019, pp. 135–156.
- [15] S.K. Bhadoria, R.G. Burela, Analytical and computational study of compressible neo-hookean model using vam for two types of global warping constraints, *International Journal of Non-Linear Mechanics*, 160 (2024) 104652.
- [16] S.K. Bhadoria, R.G. Burela, Asymptotically correct 3d displacement of the Mooney–Rivlin model using vam, *Thin-Walled Structures*, 195 (2024) 111358.
- [17] K.C. Le, An asymptotically exact first-order shear deformation theory for functionally graded plates, *International Journal of Engineering Science*, 190 (2023) 103875.
- [18] K.C. Le, B.D. Nguyen, Polygonization: Theory and comparison with experiments, *International Journal of Engineering Science*, 59 (2012) 211–218.
- [19] K.C. Le, B.D. Nguyen, On bending of single crystal beam with continuously distributed dislocations, *International Journal of Plasticity*, 48 (2013) 152–167.
- [20] K.C. Le, L.T.K. Nguyen, *Energy methods in dynamics*, Springer, 2014.
- [21] K.C. Le, J.-H. Yi, An asymptotically exact theory of smart sandwich shells, *International Journal of Engineering Science*, 106 (2016) 179–198.
- [22] K.C. Le, An asymptotically exact theory of functionally graded piezoelectric shells, *International Journal of Engineering Science*, 112 (2017) 42–62.

- [23] K.C. Le, Introduction to Micromechanics, Nova Science, 2 edition, 2020.
- [24] K.C. Le, T.M. Tran, Asymptotically exact theory of fiber-reinforced composite beams, *Composite Structures*, 244 (2020) 112279.
- [25] K.C. Le, T.M. Tran, Asymptotically exact theory of functionally graded elastic beams, *International Journal of Engineering Science*, 209 (2025) 104214.
- [26] T. Belytschko, H. Stolarski, W.K. Liu, N. Carpenter, J.S.J. Ong, Stress projection for membrane and shear locking in shell finite elements, *Computer Methods in Applied Mechanics and Engineering*, 51 (1-3) (1985) 221–258.
- [27] M.L. Bucalem, K.-J. Bathe, Finite element analysis of shell structures, *Archives of Computational Methods in Engineering*, 4 (1997) 3–61.
- [28] K.-U. Bletzinger, M. Bischoff, E. Ramm, A unified approach for shear-locking-free triangular and rectangular shell finite elements, *Computers & Structures*, 75 (3) (2000) 321–334.
- [29] K.C. Le, *Vibrations of Shells and Rods*, Springer, Berlin, 1999.
- [30] O.C. Zienkiewicz, R.L. Taylor, J.M. Too, Reduced integration technique in general analysis of plates and shells, *International Journal for Numerical Methods in Engineering*, 3 (2) (1971) 275–290.
- [31] E. Onate, E. Hinton, N. Glover, Techniques for improving the performance of Ahmad shell elements, in: *Proc. Int. Conf. on Applied Numerical Modelling*, Pentech Press, Madrid, 1978, pp. 30–53.
- [32] T.J.R. Hughes, M. Cohen, M. Haroun, Reduced and selective integration techniques in the finite element analysis of plates, *Nuclear Engineering and Design*, 46 (1) (1978) 203–222.
- [33] T.J.R. Hughes, *The Finite Element Method: Linear Static and Dynamic Finite Element Analysis*, Courier Corporation, 2012.
- [34] T.J.R. Hughes, T. Tezduyar, Finite elements based upon Mindlin plate theory with particular reference to the four-node bilinear isoparametric element, *J. Appl. Mech.*, 48 (1981) 587–596.

- [35] A.F. Saleeb, T.Y. Chang, W. Graf, S. Yingyeunyong, A hybrid/mixed model for non-linear shell analysis and its applications to large-rotation problems, *International Journal for Numerical Methods in Engineering*, 29 (2) (1990) 407–446.
- [36] J.C. Simo, M.S. Rifai, A class of mixed assumed strain methods and the method of incompatible modes, *International Journal for Numerical Methods in Engineering*, 29 (8) (1990) 1595–1638.
- [37] N. Büchter, E. Ramm, D. Roehl, Three-dimensional extension of non-linear shell formulation based on the enhanced assumed strain concept, *International Journal for Numerical Methods in Engineering*, 37 (15) (1994) 2551–2568.
- [38] F. Koschnick, M. Bischoff, N. Camprubí, K.-U. Bletzinger, The discrete strain gap method and membrane locking, *Computer Methods in Applied Mechanics and Engineering*, 194 (21-24) (2005) 2444–2463.
- [39] T. Nguyen-Thoi, P. Phung-Van, C. Thai-Hoang, H. Nguyen-Xuan, A cell-based smoothed discrete shear gap method (cs-dsg3) using triangular elements for static and free vibration analyses of shell structures, *International Journal of Mechanical Sciences*, 74 (2013) 32–45.
- [40] J.F. Caseiro, R.A.F. Valente, A. Reali, J. Kiendl, F. Auricchio, R.J. Alves de Sousa, On the assumed natural strain method to alleviate locking in solid-shell NURBS-based finite elements, *Computational Mechanics*, 53 (2014) 1341–1353.
- [41] B. Oesterle, E. Ramm, M. Bischoff, A shear deformable, rotation-free isogeometric shell formulation, *Computer Methods in Applied Mechanics and Engineering*, 307 (2016) 235–255.
- [42] M. Lavrenčič, B. Brank, Hybrid-mixed low-order finite elements for geometrically exact shell models: Overview and comparison, *Archives of Computational Methods in Engineering*, 28 (2021) 3917–3951.
- [43] K.C. Le, H.-G. Bui, Asymptotically accurate and locking-free finite element implementation of first order shear deformation theory for plates, *Computers & Structures*, 298 (2024) 107387.

- [44] J. Kiendl, Y. Bazilevs, M.C. Hsu, R. Wüchner, K.U. Bletzinger, The bending strip method for isogeometric analysis of Kirchhoff–Love shell structures comprised of multiple patches, *Computer Methods in Applied Mechanics and Engineering*, 199 (37) (2010) 2403–2416.
- [45] M.J. Borden, M.A. Scott, J.A. Evans, T.J.R. Hughes, Isogeometric finite element data structures based on Bézier extraction of NURBS, *International Journal for Numerical Methods in Engineering*, 87 (1-5) (2011) 15–47.
- [46] P. Dadvand, R. Rossi, E. Oñate, An Object-oriented Environment for Developing Finite Element Codes for Multi-disciplinary Applications, *Archives of Computational Methods in Engineering*, 17 (3) (2010) 253–297.
- [47] A.E.H. Love, *A treatise on the mathematical theory of elasticity*, Cambridge University Press, 2013.